Planetary Atmospheres: Chemistry & Composition

Channon Visscher
Dordt University, Sioux Center, Iowa 51250, USA
Space Science Institute, Boulder, Colorado, 80301, USA
channon.visscher@dordt.edu

preprint for *The Oxford Research Encyclopedia of Planetary Science*

October 26, 2022

Abstract

The observed composition of a planetary atmosphere is the product of planetary formation and evolution, including the chemical and physical processes shaping atmospheric abundances into the present day. In our solar system, the gas giant planets Jupiter, Saturn, Uranus, and Neptune possess massive molecular envelopes consisting mostly of H_2 and He along with various minor amounts of heavy elements such as C, N, and O (present as CH_4, NH_3, and H_2O, respectively) and numerous additional minor species. The terrestrial planets Venus, Earth, and Mars each possess a relatively thin atmospheric envelope surrounding a rocky surface. The atmospheres of Mars and Venus are characterized by abundant CO_2 with a small amount of N_2, whereas the atmosphere of the Earth is dominated by N_2 and O_2. Such differences provide clues to the divergent pathways of atmospheric evolution.

Numerous closely coupled physical and chemical processes give rise to the abundances observed in the planetary atmospheres of our solar system. These processes include the maintenance of thermochemical equilibrium, reaction kinetics, atmospheric transport, photochemistry, condensation (including cloud formation) and vaporization, deposition and sublimation, diurnal and seasonal effects, greenhouse effects, surface-atmosphere reactions, volcanic activity, and (in the case of Earth) biogenic and anthropogenic sources. Our present understanding of the chemical composition of planetary atmospheres is the result of over a century of observations, including ground-based, space-based, and *in-situ* measurements of the major, minor, trace, and isotopic species found on each planet. These observations have been accompanied by experimental studies of planetary materials and the development of theoretical models to identify the key processes shaping atmospheric abundances observed today.

Keywords: planetary atmosphere; ground-based; space observation; terrestrial planets; giant planets; chemical composition; troposphere; stratosphere; sources and sinks

1 Observations of planetary atmospheres before the era of spacecraft exploration

Our understanding of the composition and chemical processes of planetary atmospheres has paralleled the development of planetary science as a modern field of study. The earliest efforts at characterizing planetary environments were based upon a combination of descriptive telescopic observations (including those of Robert Hooke and Giovanni Cassini in the 1660s) accompanied by experiences of our own terrestrial atmosphere. By the late 18th century, the existence of atmospheres on other planets was demonstrated by Mikhail Lomonosov and Thorbern Bergman during the 1761 transit of Venus (e.g., see Marov 2004). Improving telescopic observations provided evidence of atmospheric processes akin to those on the Earth, such as found in William Herschel's description of seasonal cycles in the polar regions of Mars (e.g., Herschel 1784).

A number of key developments in chemical spectroscopy (e.g., see Thomas 1991) in the 19th century provided the methods first employed toward the detection and quantification of chemical species in planetary atmospheres. By 1814, Joseph von Fraunhofer had invented the modern version of the spectroscope, which was soon put to use to explore absorption features in light from the Sun and bright stars. Early spectroscopic observations of the planets were described by William Huggins and Angelo Secchi in the 1860s and 1870s, based upon visual observations of major spectral features at visible wavelengths (e.g., Huggins 1867; Dunham 1949) and by the 1870s the ongoing development of astro-photographic techniques led to the first spectrographs capable of recording planetary reflection spectra (e.g., Draper 1877, 1879; Huggins 1876). Meanwhile, the study of atomic and molecular spectroscopy had also continued to advance, led by the pioneering work of Kirchoff and Bunsen (Kirchhoff 1860; Kirchhoff & Bunsen 1860) on visible and ultraviolet spectra, followed by the development of infrared spectroscopy. By the early 20th century, the characteristic absorption features of numerous molecules had been measured, paving the way for their chemical identification and quantification in the spectra of planetary atmospheres.

A snapshot of our understanding of planetary atmospheres by the mid-20th century was summarized in *The Atmospheres of the Earth and Planets*, a collection papers edited by Gerard Kuiper (Kuiper 1952). Although ground-based observations of the planets are hampered by telluric absorption features (mitigated by using spectral features Doppler-shifted by relative planetary motions, or by comparison against solar or lunar spectra; e.g., see Slipher 1904), by the mid-20th century the bulk composition of each planetary atmosphere had been approximated from spectroscopic observations along with measurements of other properties, such as planetary density. Moreover, measurements of atmospheric scale heights from stellar occultation observations (e.g., Fabry 1929; Baum & Code 1953) provided information about the mean molecular weight of planetary atmospheres, yielding additional constraints on chemical composition. At the dawn of the era of spacecraft exploration (marked by the 1962 flyby of Venus by *Mariner 2*, and in the outer solar system by the 1973 flyby of Jupiter by *Pioneer 10*), ground-based observations had been used to detect atmospheric species on Venus (CO_2), Mars (CO_2, H_2O), Jupiter (H_2, CH_4, NH_3), Saturn (H_2, CH_4), Uranus (H_2, CH_4), and Neptune (H_2, CH_4). In addition to these discoveries, numerous species continued to be found and analyzed in the terrestrial atmosphere by various methods, including chemical analysis, infrared spectroscopy, mass spectroscopy, and gas chromatography.

The advent of the space age was revolutionary for our modern understanding of planetary atmospheres, providing closer and clearer planetary views via flybys or orbiters and (in some cases) *in-situ* measurements (often via gas chromatography and/or mass spectrometry) from landers, rovers, and atmospheric entry probes. This spacecraft exploration has been accompanied by ongoing improvements in ground-based observational data, a growing suite of instrumental methods, the increasing availability of experimental results that describe the properties and behavior of planetary materials, and the continuing development of our theoretical understanding of key chemical processes shaping the composition of the atmospheres in our solar system.

2 The diversity of atmospheres in the solar system

A diverse range of planetary and satellite atmospheres can be found across the solar system, from tenuous atmospheres of "airless" worlds to the massive fluid envelopes of the gas giants. For example, the tenuous atmospheres of satellites and planets such as the Moon and Mercury behave as surface-bound exospheres with typical surface pressures of $\sim 10^{-14}$ bar (Moon) up to $\sim 10^{-12}$ bar (Mercury), consisting of H, He, O, Ne, and Ar and metal atoms (such as Na, K, Ca, and Mg) supplied by the solar wind, micrometeorite bombardment, impact vaporization, and surface sputtering (e.g., Potter & Morgan 1985, 1986; Killen & Ip 1999; Killen *et al.* 2007; Wurz *et al.* 2007; Domingue *et al.* 2007; Vervack *et al.* 2010; Merkel *et al.* 2017). Jupiter's moon Io has an SO_2-rich atmosphere supplied by volcanism and sublimation, with surface pressures up to $\sim 10^{-7}$ bar (McGrath *et al.* 2004; Lellouch 2005). The atmospheres of Pluto and Neptune's moon Triton have surface pressures of $\sim 10^{-6}$ bar and consist of N_2 with minor amounts of CH_4 and CO, subject to vapour pressure equilibrium and seasonal exchange with surface ices (e.g., Yelle & McGrath 1996; Elliot *et al.* 1998; Yelle & Elliot 1997; Summers *et al.* 1997; Spencer *et al.* 1997; Lellouch *et al.* 2010; Zalucha & Cook 2019). Other icy satellites in the outer solar system have tenuous atmospheres (e.g., Europa, Ganymede, Callisto, Enceladus, Rhea, Dione) supplied by surface sputtering, the sublimation of surface ices, or plumes. In contrast, Saturn's moon Titan has a substantial N_2-rich atmosphere with CH_4 and other hydrocarbons that may produce hazes and/or condense as liquids at the surface conditions of 94 K and 1.5 bar (see review in Hörst 2017). The terrestrial planets Venus, Earth, and Mars have significant, long-lived atmospheres surrounding rocky surfaces. The atmospheres of Venus and Mars are characterized by abundant CO_2 whereas the atmosphere of Earth is dominated by N_2 and O_2. The giant planets Jupiter, Saturn, Uranus, and Neptune possess massive, hydrogen-rich atmospheric envelopes, with minor amounts of heavy elements (i.e., heavier than He) such as C, N, and O, present respectively as CH_4, NH_3, and H_2O, along with numerous additional species.

The range of planetary and satellite atmospheres observed in the solar system is a natural consequence of divergent formation and evolutionary scenarios. For example, the hydrogen-rich envelopes of the giant planets (Jupiter, Saturn, Uranus, Neptune) suggest that their atmospheres were mostly captured from the protoplanetary disk during their initial formation, while there was still enough H and He gas in the disk available for significant accretion (e.g., see Lissauer 1993; Lunine *et al.* 2004; Taylor *et al.* 2004; Chambers 2014). Given their resemblance to a "protosolar-composition" gas, these atmospheres have traditionally been labeled *primary atmospheres*. For the smaller terrestrial planets (Venus, Earth, Mars), the relative lack of H and He and very low noble gas abundances suggest that atmospheric volatiles initially accreted or captured during planetary formation have been lost to escape. These so-called *secondary atmospheres* appear to be the result of impact accretion and outgassing (primarily via volcanic activity) of volatile-rich material (e.g., see reviews in Atreya *et al.* 1989) and numerous other sources and sinks operating over long timescales. The present-day atmospheres thus represent a record of the major processes that have shaped planetary formation and evolution throughout the history of the solar system.

This review summarizes the atmospheric chemistry and composition of solar system planets that have significant atmospheres, considering first the terrestrial planets Venus, Earth, Mars, followed by the gas giant planets Jupiter, Saturn, Uranus, and Neptune. For each of these planets, measurements of the atmospheric abundances are provided, along with a brief discussion of the key chemical processes that shape atmospheric composition.

3 The physical properties of planetary atmospheres

The structure of a planetary atmosphere (including, for example, the temperature, pressure, or molecular number density as a function of altitude) defines the conditions for atmospheric chemistry, and is likewise shaped by atmospheric composition and chemical processes. It is thus useful to consider the relevant physical parameters (see properties listed in Table 1) and structural relationships (e.g., Chamberlain & Hunten 1989; Frederick 2008) that provide the context for chemical processes in planetary atmospheres.

Table 1: Physical Properties of Planetary Atmospheres

Parameter	Venus	Earth	Mars	Jupiter	Saturn	Uranus	Neptune
semi-major axis (AU)	0.723	≡1.000	1.523	5.205	9.582	19.201	30.047
solar constant (W/m^2)	2602.0	1361.1	586.5	50.2	14.8	3.7	1.5
equilibrium temperature (K)	227	254	210	110	81	58	47
surface/reference temperature (K)	740	288	214	165.0	134.8	76.4	71.5
surface/reference pressure (bar)	95.6	1.013	0.00636	≡1.0	≡1.0	≡1.0	≡1.0
surface/reference gravity (m/s^2)	8.87	9.798	3.71	24.79	10.44	8.87	11.15
mean molecular mass (amu)	43.45	28.97	43.34	2.30	2.34	2.63	2.72
atmospheric scale height (km)	15.9	8.4	10.8	24.1	47.3	27.7	20.0
dry adiabatic lapse rate (K/km)	7.8	9.8	5.0	2.2	1.0	1.1	1.4
tropopause temperature (K)	214	216	140	104	85	54	52
tropopause pressure (mbar)	200	220	0.01	140	80	100	200

Mean molecular mass information calculated from atmospheric abundances; outer planet tropopause info from Chamberlain & Hunten (1989); Venus tropopause info from Limaye *et al.* (2018). The equilibrium temperature is a blackbody approximation that parameterises thermal balance with the solar energy absorbed by the planet; the surface/reference temperature also includes contributions from a greenhouse effect and/or a heat flux from the planetary interior.

For terrestrial planets, the surface pressure provides a measure of the total mass of the overlying atmosphere:

$$P = \frac{m_a g}{A} = \sigma_a g, \tag{1}$$

where P is the pressure (Pa), g is the surface gravity (m s^{-2}), A is the surface area of the planet (m^2), m_a is the total mass (kg), and σ_a is the column mass (kg m^{-2}) of the atmosphere. In general, all planetary atmospheres may be assumed to be in hydrostatic equilibrium. The decrease in pressure with altitude (as the mass of the overlying atmosphere decreases) can thus be expressed by

$$dP = -\rho g dz, \tag{2}$$

where P is the pressure (Pa), ρ is the density (kg m^{-3}), g is the gravity (m s^{-1}), and z is the altitude (m). Assuming molar quantities (e.g., $n = 1$ and $V = V_m$) in the ideal gas law ($PV = nRT$), the atmospheric density is defined by

$$\rho = \frac{\mu}{V} = \frac{\mu P}{RT}, \tag{3}$$

where μ is the mean molecular weight (kg mol^{-1}), V is volume (m^{-3}), P is the pressure (Pa), R is the gas constant (8.314 J K^{-1} mol^{-1}), and T is the temperature (K). Substitution of the ideal gas law into the hydrostatic equation yields

$$dP = -\frac{\mu g}{RT} P dz. \tag{4}$$

Integrating from some reference pressure $P_\circ$ at altitude $z = 0$ to some pressure P at altitude z gives an expression that describes the variation of pressure as a function of altitude:

$$P = P_\circ e^{-z/H}, \tag{5}$$

where H is the *atmospheric scale height* defined by

$$H = \frac{RT}{\mu g}, \tag{6}$$

describing the altitude over which there is a $1/e$ decrease in the atmospheric pressure and density. Comparative atmospheric scale heights are provided in Table 1. Variations in pressure and density with altitude thus depend upon the gravity, the mean molecular weight of atmospheric species, and the atmospheric temperature gradient. The change in temperature as a function of altitude is known as the *lapse rate* (Γ, K m^{-1} or more commonly K km^{-1}):

$$\Gamma = -\frac{dT}{dz}. \tag{7}$$

A dry adiabatic lapse rate (i.e., the scenario where no condensation is occurring) can be approximated from combining a form of the first law of thermodynamics ($C_p dT = V dP$) with the hydrostatic and density expressions above ($dP = -\rho g dz$ and $\rho = \mu/V$) to give

$$C_p dT = -V \rho g dz = -\mu g dz \tag{8}$$

where C_p is the average molar heat capacity of the atmospheric gas (J K^{-1} mol^{-1}) based upon its chemical composition. Combining this expression with the hydrostatic relation in equation (4) and integrating from $P_\circ \rightarrow P$, and $T_\circ \rightarrow T$, the profile of an adiabatic troposphere is thus given by

$$P = P_\circ \left(T/T_\circ\right)^{C_p/R}, \tag{9}$$

where $P_\circ$ and $T_\circ$ refer to some reference point in the atmosphere (e.g., 288 K and 1 bar on Earth). Taken together, equations (1)-(9) demonstrate the importance of the closely coupled relationships between pressure and density, thermal structure, planetary gravity, and chemical composition.

The abundances of individual atmospheric gases are typically reported as a mole fraction or volume mixing ratio, defined as the ratio of the partial pressure of some gas i (P_i) relative to the total atmospheric pressure (P). Depending upon relative abundance, this value may be reported as

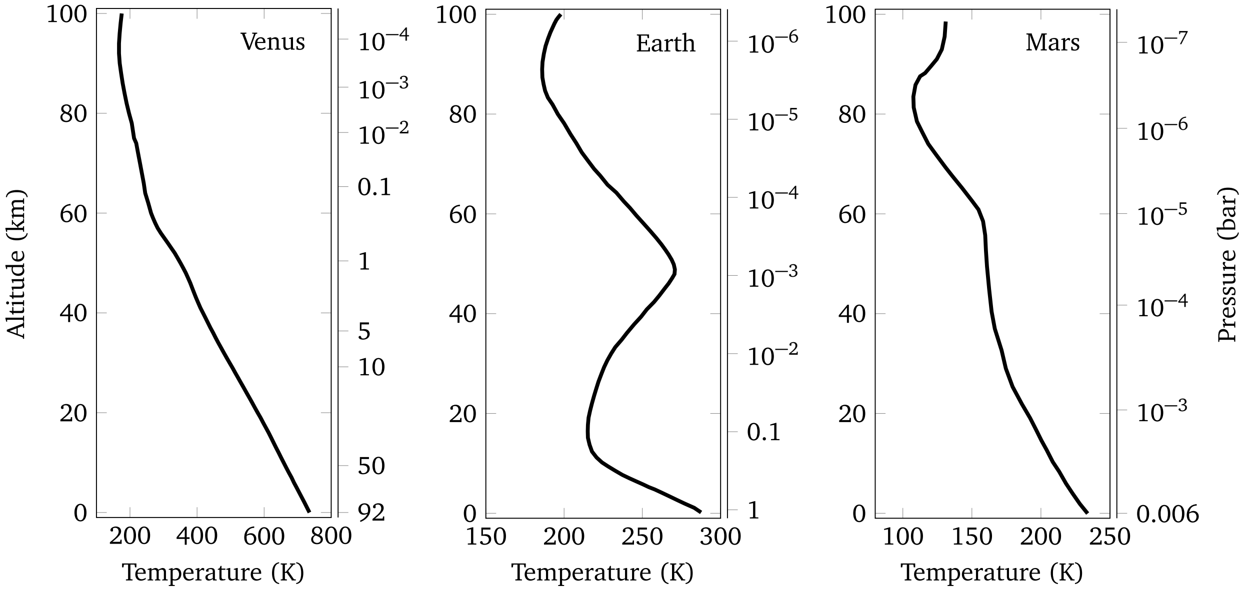

Figure 1: Atmospheric profiles for Venus, Earth, Mars from 0-100 km altitude (note different scales for temperature and pressure). Sources: U.S. Standard Atmosphere (NOAA/NASA/USAF 1976); Venus International Reference Atmosphere (VIRA; Seiff *et al.* 1985); Mars lander/rover entry data (e.g., Holstein-Rathlou *et al.* 2016; Schofield *et al.* 1997; Seiff & Kirk 1977)

percent (%), parts per million (ppm), parts per billion (ppb), or parts per trillion (ppt). The partial pressure can also be used with the ideal gas law ($n_i = P_i V / RT$) to determine the molar (e.g., mol cm^{-3}) or molecular (e.g., molecules cm^{-3}) number density of each atmospheric constituent.

4 Terrestrial planet atmospheres

The atmospheres of the terrestrial planets (Venus, Earth, and Mars) are relatively thin layers of gas surrounding rocky planetary surfaces. For example, over 99% of the mass of the Earth's atmosphere resides below an altitude of 40 km, compared to a mean planetary radius of 6371 km. The atmospheric profiles of Venus, Earth, and Mars to an altitude of 100 km are shown in Figure 1. These profiles are derived from the Venus International Reference Atmosphere (VIRA; Seiff *et al.* 1985) based upon the *Pioneer Venus* orbiter and atmospheric probes and the *Venera* 10, 12, and 13 descent craft for Venus; the U.S. Standard Atmosphere for the Earth (NOAA/NASA/USAF 1976); and atmospheric entry data derived from the *Mars Science Laboratory* (Holstein-Rathlou *et al.* 2016), *Mars Pathfinder* (Schofield *et al.* 1997), and the *Viking* landers (Seiff & Kirk 1977) for Mars.

The atmospheric mass ratios and abundances of selected volatiles on the terrestrial planets (expressed as gram per gram of object) are summarized in Figure 2. The terrestrial planet atmospheres observed today appear to be secondary atmospheres mainly produced by the release of volatiles during impact accretion and subsequent out-gassing via volcanic activity. However, numerous

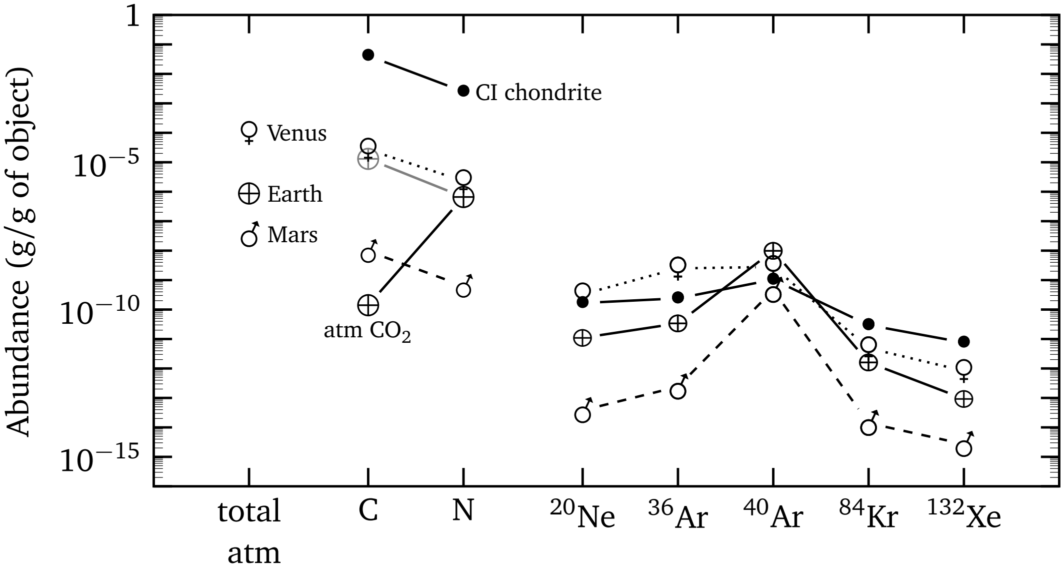

Figure 2: After Pepin (1991, 2006) and Pollack & Black (1982) using CI chondrite abundances from Lodders (2020) with the CI chondrite ^{40}Ar/^{36}Ar abundance ratio estimated from Mazor *et al.* (1970). Planetary atmosphere (g/g) abundances calculated from Tables 2-4 using isotope ratios from Pollack & Black (1982) along with measurements summarized in Fegley (2014) for Venus and reported by Mahaffy *et al.* (2013) for Mars. The abundance of atmospheric carbon as CO_2 is 10^{-10} g/g for the Earth whereas, the total carbon inventory in the Earth's lithosphere (indicated in grey) corresponds to $\sim 10^{-5}$ g/g.

source and sink processes have shaped terrestrial atmospheric compositions throughout the history of the solar system, including capture from the protoplanetary disk, impact accretion, volcanic outgassing, impact erosion, stripping from the solar wind, atmospheric escape, surface-atmospheric interactions, exchange with interior reservoirs, metamorphism, weathering, and biological activity.

The relative lack of any remnant primordial atmosphere is implied by the behavior of the abundant light gases H_2 and He and the very low atmospheric concentrations of the nonradiogenic noble gases (cf. Trieloff 2017). For example, H_2 and He are expected to comprise a significant component of any atmosphere initially captured from the protoplanetary disk, but these light gases are readily lost from the low-gravity environments of the terrestrial planets. However, the production of a secondary atmosphere is not simply the loss of some initial H_2 and He inventory, as the heavier (and thus less subject to thermal escape) noble gases Ne, Ar, Kr, and Xe are also present at abundances much lower than expected for a primordial (or protosolar-composition) atmosphere. The presence of a secondary atmosphere is further supported by the relatively high abundance of radiogenic or "outgassed" noble gas isotopes such as ^{40}Ar, produced from the radioactive decay of accreted ^{40}K. Modern studies have continued to explore how these volatile element and isotopic abundance patterns provide clues about the origin and evolution of terrestrial planet atmospheres (e.g., see Atreya *et al.* 1989; Pepin 1991; Marty 2012; Halliday 2013; Avice & Marty 2020; Lammer *et al.* 2021, and references therein)

4.1 Venus

The atmosphere of Venus is notable for its high surface temperature and pressure (740 K and 95.6 bar at the modal radius of 6051.4 km), and consists of 96.5% CO_2 with 3.5% N_2 along with smaller amounts of SO_2, H_2O, CO, OCS, the noble gases, and other reactive species. The composition of the lower atmosphere of Venus is summarized in Table 2.

Table 2: Composition of the lower atmosphere of Venus

Gas	Abundance	Source	Sink
CO_2	96.5%	volcanic outgassing; carbonates	photochemistry;
N_2	3.5%	volcanic outgassing	NO_x formation by lightning
$SO_2^\dagger$	150 ppm	volcanic outgassing; S oxidation	H_2SO_4 clouds; sulfates, sulfides
^{36}Ar	31 ppm	volcanic outgassing; primordial	none
^{40}Ar	30 ppm	volcanic outgassing; ^{40}K decay	none
$H_2O^\dagger$	30 ppm	volcanic outgassing	H escape; oxidation of Fe^{+2}
$CO^\dagger$	17 ppm	CO_2 photolysis	photooxidation; OCS formation
He	9 ppm	volcanic outgassing	escape
Ne	7 ppm	volcanic outgassing; primordial	none
$OCS^\dagger$	4.4 ppm	volcanic outgassing; CO sulfurization	conversion to SO_2; S-bearing minerals
$H_2S^\dagger$	3 ppm	volcanic outgassing	conversion to SO_2; S-bearing minerals
HCl	0.4 ppm	volcanic outgassing	Cl-bearing mineral formation
$SO^\dagger$	20 ppb	photolysis of SO_2	photolysis; oxidation
$S_{1-8}^\dagger$	20 ppb	polysulfur cycle; surface reactions	conversion to SO_2
Kr	$\sim$25 ppb^a	volcanic outgassing; primordial	none
$H_2SO_4^\dagger$	4-10 ppm	oxidation of S-bearing gases	cloud formation; dehydration to SO_3
Xe	$\sim$7 ppb^a	volcanic outgassing; primordial	none
HF	5 ppb	volcanic outgassing	F-bearing mineral formation

Table adapted after abundances and sources/sinks compiled in Lodders & Fegley (1998) and Fegley (2014); cf. von Zahn *et al.* (1983); Moroz & Zasova (1997); Bézard & de Bergh (2007); Zolotov (2019); Vandaele (2020). ^{a}Model-dependent estimate; †Abundances are altitude-dependent and the abundance measurement at the lowest available altitude is listed here; see von Zahn *et al.* (1983); Fegley (2014); Marcq *et al.* (2018); Vandaele (2020) for details.

In the 1930s, the spectroscopic detection of large quantities of carbon dioxide in Venus' atmosphere (Adams & Dunham 1932; Adel & Slipher 1934) led Ruper Wildt to predict surface temperatures higher than the boiling point of water (Wildt 1940). This prediction was later confirmed by ground-based and *Mariner 2* microwave observations of Venus' thermal emission (Lilley 1961; Barath *et al.* 1964). The high surface temperatures are maintained by an intense greenhouse effect. A bright and thick global layer of sulfuric acid clouds (measured by the *Pioneer Venus* large probe to be distributed between altitudes of 48-65 km) absorbs and reflects incident sunlight so effectively that the average incoming visible flux reaching the surface is significantly lower than that for the Earth: less than 4% of the incident shortwave flux at the top of the Venus' atmosphere is absorbed at Venus' surface (e.g., see Read *et al.* 2016). However, infrared emission from the surface and the sub-cloud atmosphere is very effectively absorbed by abundant CO_2 ($\sim$92 bar) along with SO_2 and other greenhouse gases.

In general, the observed chemical composition of Venus' atmosphere is a reflection of volcanic outgassing, high surface and crustal temperatures, and surface-atmosphere interactions. From a chemical standpoint it is convenient to divide the atmosphere into the region above the clouds, where UV-driven photochemistry dominates, and the sub-cloud region, where thermochemistry dominates. Photochemical models have thus played an important role in our understanding the chemistry of the upper atmosphere (e.g., see Yung & Demore 1982; Yung & DeMore 1999), and recent models also explore the role of thermochemical equilibria and diffusive atmospheric mixing (e.g., Krasnopolsky 2006, 2012; Bierson & Zhang 2020). Near the cloud layers and above, CO_2 in Venus' atmosphere is readily destroyed by photolysis:

$$\mathrm{CO_2} \xrightarrow{h\nu} \mathrm{CO} + \mathrm{O}. \tag{10}$$

The reverse reaction $\mathrm{CO} + \mathrm{O} \xrightarrow{\mathrm{M}} \mathrm{CO_2}$ is spin forbidden and therefore slow, and recombination of O is more likely to result in O_2. Without an efficient production route, CO_2 would thus be completely removed from Venus' atmosphere in about 5 million years. Moreover, a reaction important for Mars and Earth,

$$\mathrm{CO} + \mathrm{OH} \rightarrow \mathrm{CO_2} + \mathrm{H}, \tag{11}$$

is not effective given insufficient OH production from H_2O, which is relatively scarce on Venus. Instead, a number of plausible catalytic reformation pathways have been proposed to resolve this stability problem, involving SO_x, NO_x, and/or ClO_x species. For example, Prinn (1971) first pointed out the potential importance of ClO_x for catalysing CO_2 formation on Venus. Near the cloud tops, atomic Cl is produced by the photolysis of HCl:

$$\mathrm{HCl} \xrightarrow{h\nu} \mathrm{Cl} + \mathrm{H} \tag{12}$$

which readily reacts with CO to initiate a catalytic cycle than can efficiently recycle CO back into

CO_2:

$$\mathrm{Cl} + \mathrm{CO} \xrightarrow{\mathrm{M}} \mathrm{ClCO} \tag{13}$$

$$\mathrm{ClCO} + \mathrm{O_2} \xrightarrow{\mathrm{M}} \mathrm{ClCOO_2} \tag{14}$$

$$\mathrm{ClCOO_2} + \mathrm{O} \rightarrow \mathrm{CO_2} + \mathrm{O_2} + \mathrm{Cl} \tag{15}$$

$$\mathrm{O} + \mathrm{CO} \rightarrow \mathrm{CO_2}. \tag{net, scheme 1}$$

Likewise, sulfur oxides (SO_x) are readily photolyzed and serve as a source of atomic O in the cycle (e.g., Winick & Stewart 1980; Yung & Demore 1982; Yung & DeMore 1999):

$$\mathrm{SO_2} \xrightarrow{h\nu} \mathrm{SO} + \mathrm{O} \tag{16}$$

$$2\mathrm{SO} \rightarrow \mathrm{SO_2} + \mathrm{S} \tag{17}$$

$$\mathrm{S} + \mathrm{O_2} \rightarrow \mathrm{SO} + \mathrm{O} \tag{18}$$

$$\mathrm{O_2} \rightarrow 2\mathrm{O}. \tag{net, scheme 2}$$

The above schemes can be combined in a larger cycle that results in the recycling of CO_2 and the formation of sulfuric acid via the series of reactions:

$$\mathrm{O} + \mathrm{CO} \rightarrow \mathrm{CO_2} \tag{net, scheme 1}$$

$$\mathrm{O_2} \rightarrow 2\mathrm{O} \tag{net, scheme 2}$$

$$\mathrm{O} + \mathrm{SO_2} \xrightarrow{\mathrm{M}} \mathrm{SO_3} \tag{19}$$

$$\mathrm{H_2O} + \mathrm{SO_3} \xrightarrow{\mathrm{M}} \mathrm{H_2SO_4} \tag{20}$$

$$\mathrm{CO} + \mathrm{O_2} + \mathrm{SO_2} + \mathrm{H_2O} \rightarrow \mathrm{H_2SO_4} + \mathrm{CO_2}. \tag{net, scheme 3}$$

The identification of the cloud composition as sulfuric acid was proposed by Sill (1972) and Young (1973) based upon the spectral properties and refractive index of the cloud layers, along with the need for a desiccating agent that could remove H_2O. A sulfuric acid composition could also explain the apparent lack of SO_2, which was not detected until 1979 by ground-based UV observations (Barker 1979). At higher temperatures below the cloud base (48 km), sulfuric acid thermally decomposes via the reaction:

$$\mathrm{H_2SO_4} \rightarrow \mathrm{H_2O} + \mathrm{SO_3}, \tag{21}$$

consistent with radio occultation observations that show a drop off in the H_2SO_4 vapour abundance below 48 km (Kolodner & Steffes 1998; Bézard & de Bergh 2007).

The high temperatures and obscuring cloud layers have made the lower atmosphere difficult to observe. A handful of *in-situ* measurements (via gas chromatography and/or mass spectroscopy) of the lower atmosphere were made by the *Pioneer-Venus* probes, the *Venera 11-12* descent craft, and the *Venera 13-14* and *Vega 1-2* landers. However, on the *Pioneer-Venus* large probe the leak inlet for the mass spectrometer was apparently blocked by a cloud droplet from 50-30 km and possible insulation failure caused instruments to fail at 12.5 km, whereas the *Venera* and *Vega* landers did not return gas chromatograph data from below 12 km. More recently, night-side thermal emission in an infrared spectra window (in between CO_2 lines near 1 μm), first detected by Allen & Crawford (1984), has allowed for additional measurements in the lower atmosphere below the clouds (e.g, see Marcq *et al.* 2006; Bézard & de Bergh 2007; Arney *et al.* 2014). However, the chemical abundances of the near-surface atmosphere remain uncertain, particularly for species that demonstrate altitude dependence. Theoretical modeling has thus served as an important tool for understanding chemical processes in this region of the atmosphere.

Given the high temperatures and pressures and the lack of ultraviolet flux, chemistry in the lower atmosphere is dominated by thermally-driven reactions and over long timescales may also be subject to gas-solid reactions at the surface, since 50% of the atmospheric mass resides below the 11-km summit of Maxwell Montes. A comprehensive exploration of chemical weathering and atmosphere-surface interactions can be found in Zolotov (2019); the salient points of interest for atmospheric composition are considered here. Of particular interest is the possibility that chemical equilibria of mineral phase assemblages found in the crust may regulate or "buffer" the abundance of key gases in the atmosphere. Among such reactions is that proposed by Harold Urey and Robert Mueller (Urey 1951; Mueller 1963, 1964):

$$\mathrm{CO_2(g)} + \underset{\text{wollastonite}}{\mathrm{CaSiO_3(s)}} \rightleftarrows \underset{\text{quartz}}{\mathrm{SiO_2(s)}} + \underset{\text{calcite}}{\mathrm{CaCO_3(s)}}. \tag{22}$$

If all three phases are present at equilibrium at a temperature of 740 K, this reaction yields a partial pressure of $P_{\mathrm{CO_2}} \sim 90$, roughly similar to the observed partial pressure of CO_2 near the surface. However, the operation of this buffer depends upon whether carbonates are present on the surface of Venus, which remains a subject of debate, and $CaCO_3$ is unstable toward reaction with atmospheric SO_2 at Venus surface conditions. Most of the surface carbon inventory on Earth is found in crustal rocks as carbonates, whereas the carbon inventory of Venus - lacking a comparable carbon cycle - appears to be mostly present in the atmosphere (see Figure 2). This difference in carbon reservoirs is generally ascribed to the very dry conditions on Venus, and the high D/H ratio in Venus' atmosphere (150× that of the Earth) suggests significant loss of water in the past.

The abundances of the volcanically-outgassed S-bearing species SO_2, OCS, H_2S, and S_x are altitude-dependent, shaped by photochemistry, atmospheric transport, thermally-driven reactions, and surface-atmosphere interactions as part of sulfur oxidation and polysulfur cycles (e.g., see Mills *et al.* 2007; Zhang *et al.* 2012; Marcq *et al.* 2018; Mills *et al.* 2019; Bierson & Zhang 2020;

Vandaele 2020). In the sulfur oxidation cycle, for example, the upward transport and oxidation of SO_2 and OCS leads to H_2SO_4 cloud formation. As these cloud droplets descend and evaporate, the SO_3 produced by the thermal decomposition of H_2SO_4 (Reaction 21) can recycle SO_2 and CO_2 via net reactions such as

$$\mathrm{SO_3 + CO \rightleftarrows SO_2 + CO_2}. \tag{23}$$

In the polysulfur cycle, the upward transport and photodissociation of SO_2 and OCS produces S atoms, which can react with OCS to produce S_2:

$$\mathrm{OCS + S \rightarrow CO + S_2}, \tag{24}$$

Additional thermochemical reactions involving sulfur can produce higher sulfur allotropes S_n

$$\mathrm{S_2 + S \rightleftarrows S_3}, \tag{25}$$

which have been proposed as a source of UV absorption in the upper atmosphere (Yung & DeMore 1999; Mills *et al.* 2007; Titov *et al.* 2018). Atmosphere-surface interactions may also serve as a source for sulfur species via reactions such as

$$\mathrm{4CO_2 + \underset{\text{pyrrhotite}}{3FeS(s)} \rightleftarrows \underset{\text{magnetite}}{3Fe_3O_4(s)} + 3OCS + CO}, \tag{26}$$

consistent with the increase in abundance of OCS with decreasing altitude (Marcq *et al.* 2006; Bézard & de Bergh 2007; Fegley 2014).

Sulfur dioxide, first detected in the UV spectrum of Venus (Barker 1979; Conway *et al.* 1979; Stewart *et al.* 1979), is the most abundant S-bearing gas and the third-most abundant gas Venus' atmosphere, and plays an important role in the catalytic recycling of CO_2 and sulfuric acid cloud formation. The atmospheric abundance of SO_2 is also high enough to drive surface-atmosphere reactions with carbonates (showing that $CaCO_3$ is unstable at present Venus surface conditions) and other Ca-bearing minerals via reactions such as

$$\mathrm{4\underset{\text{calcite}}{CaCO_3(s)} + 6SO_2 \rightarrow 4\underset{\text{anhydrite}}{CaSO_4(s)} + 4CO_2 + S_2} \tag{27}$$

$$\mathrm{4\underset{\text{diopside}}{MgCaSi_2O_6(s)} + 6SO_2 \rightarrow 4\underset{\text{anhydrite}}{CaSO_4(s)} + 4\underset{\text{enstatite}}{MgSiO_3(s)} + 4\underset{\text{quartz}}{SiO_2(s)} + S_2} \tag{28}$$

which serve as an atmospheric sink for SO_2. Such sulfurization reactions can thus be used to estimate the amount of volcanic outgassing necessary to maintain the observed SO_2 abundance (Fegley & Prinn 1989), and also serve as a proxy for the chemical weathering of surface rocks Zolotov (2018).

Other volcanic gases such as HCl and HF have also been detected in Venus' atmosphere

(Connes *et al.* 1967). As shown above, HCl photolysis is a source of Cl radicals in ClO_x catalytic cycles that produce CO_2. Because HCl and HF are highly reactive, surface-atmospheric buffering has been proposed to explain their abundance via gas-solid equilibria with mineral phases commonly found in alkaline basalts (which demonstrate mineralogy consistent with that inferred by surface XRF measurements), via net reaction such as (Fegley *et al.* 1997):

$$\mathrm{Al_2O_3 + NaAlSiO_3O_8 + Na_8(Al_6Si_6O_{24})Cl_2 + H_2O \rightleftarrows 9NaAlSiO_4 + 2HCl} \tag{29}$$

$$\mathrm{3SiO_2 + KMg_3AlSi_3O_{10}F_2 + H_2O \rightleftarrows KAlSi_3O_8 + 3MgSiO_3 + 2HF} \tag{30}$$

Similarly, mineral assemblages of oxides may buffer key atmospheric parameters such as the near-surface oxygen fugacity f_{O_2} (Fegley *et al.* 1997; Fegley 1997) and C-O-S equilibria, for which the f_{O_2} may regulate (for example) the near-surface H_2O/H_2, CO_2/CO, and SO_2/SO gas abundance ratios. Gas-phase equilibria in the lower atmosphere may in turn be used to indicate the relative stability of mineral phases at the surface (e.g., Zolotov 2018, 2019). Along with the near-surface near surface redox conditions and atmospheric abundances, surface mineralogy of Venus thus remains a key outstanding question for understanding chemical processes in the lower atmosphere.

4.2 Earth

The determination of the Earth's bulk atmospheric composition coincided with the chemical discovery of the molecular gases N_2 (1772), O_2 (1774), and CO_2 (1754) in the latter half of the 18th century and additional minor (e.g., Ar in 1894) and key trace species (e.g., O_3 in 1839) the in 19th and 20th centuries. The Earth's atmosphere consists of 78% N_2, 21% O_2, and 0.934% Ar with a host of minor and trace species (see Table 3), including anthropogenic species. As noted by Lodders & Fegley (2011), the increasing number of detected atmospheric species in the terrestrial atmosphere throughout the 20th century can be attributed to advances in analytical techniques and also to the appearance of anthropogenic species (such as CFCs, HCCs, HCFCs, and HFCs) that were absent prior to the 20th century. The H_2O abundance is spatially and temporally variable (up to 4%) and Earth's clouds are made of ice and/or liquid water. As an abundant and condensible species, the behavior of H_2O is of central importance for energy transfer, weather, and surface climate, and water vapour is the dominant greenhouse gas in the Earth's atmosphere. Isotopic abundance comparisons between meteorites, comets, and the oceans and atmosphere suggest that the water inventory of the Earth may have been delivered primarily via volatile-rich planetesimals during its accretion, with a possible "late veneer" of comet-like material (e.g., see Dauphas *et al.* 2000; Morbidelli *et al.* 2000; Alexander *et al.* 2012; Marty 2012; Halliday 2013; O'Brien *et al.* 2018, and references therein).

Table 3: Composition of the Atmosphere of Earth

Gas	Abundance	Source	Sink
N_2	78.08%	outgassing; bacterial denitrification	bacterial fixation; oxidation
O_2	20.95%	photosynthesis	respiration and decay; oxidative weathering
H_2O	up to 4% (variable)	evaporation	condensation
^{36}Ar	31 ppm	outgassing	none
^{40}Ar	9303 ppm	^{40}K decay; outgassing	none
CO_2	410 ppm	outgassing, combustion	photosynthesis, oceans
CO	$40-200$ ppm (variable)	photochemistry, combustion	reaction with OH
CH_4	1.8 ppm	biological, agricultural	reaction with OH
H_2	0.5 ppm	H_2O photoloysis	H atom escape
H_2O_2	$0.3-3$	photochemistry	photochemistry
^{4}He	5 ppm	outgassing, radiogenic	escape
Ne	18.18 ppm	outgassing	none
Kr	1.14 ppm	outgassing	none
Xe	87 ppb	outgassing	none
N_2O	330 ppb	biology, agriculture, combustion	stratospheric photolysis
NO_x	30-300 ppt	combustion, biology	photoloysis, photochemistry
NH_3	0.1-3 ppb	biology	wet & dry deposition
HNO_3	0.04-4 ppb	NO_x photochemistry	rainout
O_3	10-100 ppb	photochemistry	photochemistry
HCl	1 ppb	derived from sea salt aerosols; volcanism	rainout
OCS	400-520 ppt (variable)	biology, volcanism, anthropogenic	photodissociation, biology
other S-gases[a]	≤ 260 ppt	biology, combustion, volcanism	photooxidation
HCCs[b]	700 ppt	anthropogenic	reactions with OH
CFCs[c]	818 ppt	anthropogenic	stratospheric photolysis
HCFCs[d]	309 ppt	anthropogenic	reactions with OH
HFCs[e]	218 ppt	anthropogenic	reactions with OH
other halocarbons[f]	$\lesssim 200$ ppt	anthropogenic	stratospheric photolysis

Table adapted after abundances and sources/sinks compiled in Lodders & Fegley (1998), with updates for anthropogenic greenhouse gas (CO_2, CH_4, N_2O) and halocarbon trace gas abundances from the NOAA ESRL Global Monitoring Laboratory (https://www.esrl.noaa.gov/gmd/). [a] SO_2, H_2S, CS_2, $(CH_3)_2S$. [b] CH_3Cl, CH_2Cl_2, CH_2ClCH_2Cl, $CHCl_3$, C_2H_5Cl, $CHClCCl_2$, CH_3CCl_3. [c] CCl_2F_2 (CFC-12), CCl_3F (CFC-11), $C_2Cl_3F_3$ (CFC-113), $CClF_3$ (CFC-13), $C_2Cl_2F_4$ (CFC-114), C_2ClF_5 (CFC-115). [d] $CHClF_2$ (HCFC-22), $C_2H_3Cl_2F$ (HCFC-141b), $C_2H_3ClF_2$ (HCFC-142b), $CHCl_2F$ (HCFC-21) [e] CH_2FCF_3 (HFC-134a), C_2HF_5 (HFC-125), CH_2F_2 (HFC-32), $C_2H_3F_3$ (HFC-143a), $C_2H_4F_2$ (HFC-152a), C_3HF_7 (HFC-227ea), $C_4H_5F_5$ (HFC-365ma), $C_3H_2F_6$ (HFC-236fa) [f] CF_4, CCl_4, CH_3Br, CH_3I, C_2F_2, C_2Cl_4, $CBrClF_2$ (halon-1211), $CBrF_3$ (halon-1301), $C_2F_2Br_2$ (halon-2402).

Both carbon and nitrogen show fast, biologically-mediated cycles tied to slower cycles operating over geological timescales (e.g., Johnson & Goldblatt 2015). The abundant molecular nitrogen in the Earth's atmosphere – ultimately the product of geologically recent volcanic outgassing – is relatively inert due to the strength of the N≡N bond (+940 kJ/mol). However, nitrogen fixation (i.e., the conversion into ammonia, nitrates, or nitrites) can occur during combustion of fossil fuels or vegetation, or by lightning strikes that produce NO_x species. Biological fixation plays an even larger role via the bacterial nitrogenase reaction:

$$N_2 + 8H^+ + 8e^- \xrightarrow{ATP \to ADP} 2NH_4^+, \tag{31}$$

and serves as the primary sink for molecular nitrogen in the terrestrial atmosphere. The ammonium ion is converted to nitrates by nitrifying bacteria; these nitrates are then assimilated into plants or converted back into N_2 by denitrifying bacteria, completing the cycle. Even without this recycling, the large reservoir of atmospheric nitrogen would make it stable over $\sim 10^7$ years; with recycling and outgassing sources (e.g., Sano *et al.* 2001) nitrogen is abundant in Earth's atmosphere over geological timescales . A historical chronology of the development of our present-day understanding of the terrestrial nitrogen cycle can be found in the review of Galloway *et al.* (2013).

The abundances of O_2 and CO_2 in the Earth's atmosphere are coupled. The ultimate source of molecular oxygen (O_2) in the Earth's atmosphere is photosynthesis, represented by the net reaction:

$$nCO_2 + nH_2O \overset{h\nu}{\rightleftarrows} (CH_2O)_n + nO_2. \tag{32}$$

This reaction is reversible via respiration, so the accumulation of oxygen requires the burial and sequestration of organic carbon (e.g., Catling & Claire 2005; Duncan & Dasgupta 2017), a process that appears to have played a role in the gradual rise of atmospheric oxygen during the so-called Great Oxygenation Event near 2.3-2.4 Ga (e.g., see review in Lyons *et al.* 2014).

Photosynthesis also serves as a short-term sink for carbon dioxide. The CO_2 concentration shows an intra-annual variation of about 5 ppm per year corresponding to the seasonal uptake of CO_2 during northern hemisphere spring and summer (the growing season for most land vegetation on Earth), followed by the release of CO_2 back into the atmosphere during northern hemisphere fall and winter (see Figure 3). Volcanic emission of carbon dioxide is dwarfed by anthropogenic emissions (e.g., Burton *et al.* 2013), which are primarily responsible for the observed inter-annual increase of CO_2 from ∼280 ppm in 1800 to ∼410 ppm in 2020.

Other sinks for atmospheric CO_2 include the oceans, which represent a significantly larger reservoir (38,00 Gt) for carbon than the atmosphere (860 Gt; Friedlingstein *et al.* 2020). For example, rising atmospheric CO_2 concentrations from anthropogenic emission (Figure 3) drives chemical equilibria such as (cf. Archer *et al.* 2009)

$$\mathrm{CO_2} + \mathrm{H_2O} \rightleftarrows \mathrm{H_2CO_3} \tag{33}$$

$$\mathrm{H_2CO_3} + \mathrm{H_2O} \rightleftarrows +\mathrm{HCO_3^-} + \mathrm{H_3O^+} \tag{34}$$

$$\begin{array}{c}\hline \mathrm{CO_2} + 2\mathrm{H_2O} \rightleftarrows \mathrm{HCO_3^-} + \mathrm{H_3O^+},\end{array} \tag{35}$$

leading to increasing acidity (i.e., lower pH) in the Earth's oceans (e.g., Caldeira & Wickett 2003). Moreover, carbonates are precipitated by organisms to yield shell materials or produced by the chemical weathering of rocks via reactions such as

$$\mathrm{Ca^{+2}} + 2\mathrm{HCO_3^-} \rightarrow \underset{\text{calcite}}{\mathrm{CaCO_3}} + \mathrm{H_2O} + \mathrm{CO_2} \tag{36}$$

$$2\mathrm{CO_2} + \mathrm{H_2O} + \underset{\text{wollastonite}}{\mathrm{CaSiO_3}} \rightarrow \underset{\text{quartz}}{\mathrm{SiO_2}} + \mathrm{Ca^{+2}} + 2\mathrm{HCO_3^-} \tag{37}$$

$$\begin{array}{c}\hline \mathrm{CO_2} + \underset{\text{wollastonite}}{\mathrm{CaSiO_3}} \rightarrow \underset{\text{calcite}}{\mathrm{CaCO_3}} + \underset{\text{quartz}}{\mathrm{SiO_2}},\end{array} \tag{38}$$

wherein they may be subducted and returned to the atmosphere as $\mathrm{CO_2}$ via volcanic outgassing (e.g., Plank & Manning 2019). This carbonate-silicate cycle plays an important role in regulating the $\mathrm{CO_2}$ abundance (and thus planetary temperature) over geological timescales. Moreover, sedimentary carbonates and kerogen together give a lithospheric carbon reservoir of $\sim 10^8$ Gt, vastly more than is present in the hydrosphere and atmosphere. The sequestration of carbon into lithospheric reservoirs represents a key difference from Venus, for which – lacking interaction with active hydrologic and biological cycles – the carbon inventory appears to reside in the atmosphere (see Figure 2).

The temperature increase of the Earth's stratosphere (15-50 km; see Figure 1) is due to the absorption of ultraviolet sunlight by ozone. The role of ozone as the absorber responsible for the UV cutoff in the solar spectrum was first proposed by Walter Noel Hartley in 1880, based upon comparison with experimental studies of $\mathrm{O_3}$ (Hartley 1881). In their subsequent observations, Fowler & Strutt (1917) confirmed this result by identification of $\mathrm{O_3}$ absorption bands in stellar and solar spectra, and suggested that the ozone was distributed in the upper atmosphere. The invention of the Dobson spectrometer (Dobson & Harrison 1926) provided a method for regular measurement of the atmospheric column density of $\mathrm{O_3}$. In 1930, Sydney Chapman proposed a

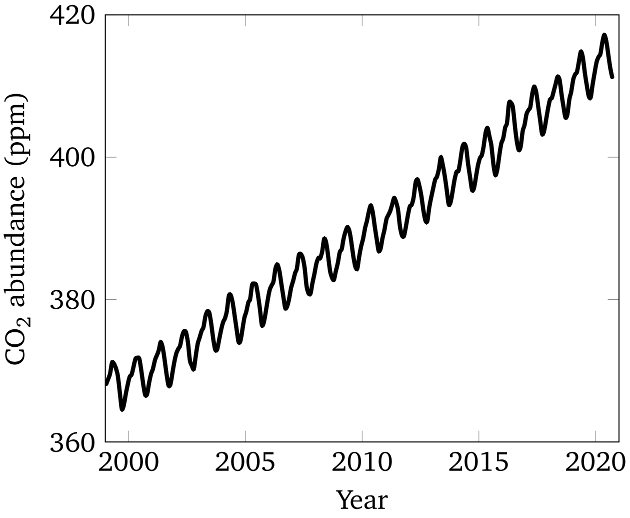

Figure 3: Abundance of CO_2 in the Earth's atmosphere from 2000-2020, showing seasonal variability and the anthropogenic inter-annual increase. Monthly data for the Mauna Loa observatory from the Scripps CO_2 Data Program (Keeling & Keeling 2017).

series of reactions to explain the behavior of ozone in the stratosphere (Chapman 1930):

$$O_2 \xrightarrow{h\nu} 2O \tag{39}$$

$$O + O_2 \xrightarrow{M} O_3 \tag{40}$$

$$O_3 \xrightarrow{h\nu} O_2 + O \tag{41}$$

$$O + O_3 \rightarrow 2O_2 \tag{42}$$

$$O_3 \rightarrow O_2 + O. \tag{net}$$

The scheme shown here omits the slow Chapman reaction $O + O \xrightarrow{M} O_2$. Moreover, the O atom produced by ozone photolysis (reaction 41) may recombine with another O_2 molecule to produce O_3 (i.e., repeating reaction 40). In this case, as noted by Yung & DeMore (1999), there is no net change in O_x for the above sequence of reactions; stratospheric ozone is thus effective at blocking ultraviolet radiation and converting it into thermal energy.

By the mid-20th century, it was recognized that oxygen-only Chapman chemistry by itself predicted stratospheric ozone abundances greater than what was observed. The search for additional O_3 loss pathways led to the discovery of key catalytic processes in the stratosphere (Bates & Nicolet 1950; Norrish & Wayne 1965a,b). Ozone is readily destroyed by reactions with free radical species such as Cl·, Br·, and OH·, and HO_x, NO_x, ClO_x, and BrO_x catalytic cycles play an important role the Earth's stratosphere.

The relative importance of a particular catalytic cycle varies with altitude and depends not only upon reaction kinetics but also upon the number of times a cycle may repeat before the catalyst is lost to other processes (i.e., the *chain rate*; see Lary 1997). In general there are two basic net reaction schemes for ozone loss. In the middle stratosphere, the dominant type of scheme is

$$X + O_3 \rightarrow XO + O_2 \tag{43}$$

$$XO + O \rightarrow X + O_2 \tag{44}$$

$$\overline{}$$

$$O + O_3 \rightarrow 2O_2, \tag{45}$$

which can begin with either reaction and where X = OH, Cl, Br, or NO. In the lower stratosphere (where the abundance of atomic O is relatively low and the abundance of O_3 is relatively high) the most effective catalytic cycle can be represented by the net reaction scheme

$$X + O_3 \rightarrow XO + O_2 \tag{46}$$

$$XO + O_3 \rightarrow X + 2O_2 \tag{47}$$

$$\overline{}$$

$$2O_3 \rightarrow 3O_2. \tag{48}$$

Additional reactions based upon this scheme can also play a role, including reactions among or between oxides (XO) such as HO_2, ClO, BrO, and NO_2 (e.g., Lary 1997):

$$XO + X'O \rightarrow X'XO_2 \tag{49}$$

$$X'XO_2 \rightarrow X' + XO_2 \tag{50}$$

$$XO_2 \rightarrow X + O_2 \tag{51}$$

$$X + O_3 \rightarrow XO + O_2 \tag{52}$$

$$X' + O_3 \rightarrow X'O + O_2 \tag{53}$$

$$\overline{}$$

$$2O_3 \rightarrow 3O_2. \tag{54}$$

Enhanced catalytic destruction of ozone occurs in polar regions, where very low temperatures and the development of the polar vortex promote the formation of polar stratospheric clouds (PSCs). Surface reactions that occur on PSC particles produce Cl radicals than can readily react with ozone (e.g., via reactions 43 and 46). For similar reasons, anthropogenic emission of halocarbons has contributed to increased catalytic destruction of stratospheric ozone. These gases are destroyed by UV photolysis such as that for CFC-12:

$$CF_2Cl_2 \xrightarrow{h\nu} CF_2Cl + Cl,$$

which produces Cl radicals in the stratosphere. Although a handful of halocarbon species (such as CH_3Cl) occur naturally, the abundances of CFCs, HCFCs, HFCs, and HCCs in Table 3 are almost entirely anthropogenically produced. CFCs are relatively inert and so survive into the stratosphere until they are destroyed by photolysis. As an alternative, many of the compounds proposed and developed to replace CFCs include hydrogen (HCFCs and HFCs). This gives them much shorter atmospheric residence times because they are subject to oxidation by OH in the troposphere (see below). In response to control measures such as the Montreal Protocols (signed in 1989), the atmospheric concentrations of the CFCs listed in Table 3 have decreased after 1995, whereas increased usage and emission has generally (aside from latitudinal and seasonal effects) increased the atmospheric concentrations of most HCFCs and HFCs.

As in the stratosphere, chemistry in the troposphere depends upon the abundances and reaction chemistry of key minor and trace species. Foremost among these is the reactive hydroxyl radical (OH), which effectively controls the atmospheric lifetimes of most minor or reactive species in the Earth's troposphere. Even though the concentration of OH is $\sim 10^6$ molecules cm^{-3} (Wayne 2000), it is the dominant oxidizing agent in the troposphere (for comparison, the number density of the Earth's atmosphere at sea level is $\sim 10^{19}$ molecules cm^{-3}). For example, a dominant loss pathway for tropospheric CO and CH_4 (and higher hydrocarbons) is rapid reaction with OH, e.g.,

$$\mathrm{OH} + \mathrm{CO} \rightarrow \mathrm{CO_2} + \mathrm{H}, \tag{55}$$

$$\mathrm{OH} + \mathrm{CH_4} \rightarrow \mathrm{CH_3} + \mathrm{H_2O}. \tag{56}$$

The primary formation pathway for hydroxyl is the the photolysis of O_3 followed by reaction of the excited oxygen atom with water:

$$\mathrm{O_3} \xrightarrow{h\nu} \mathrm{O_2^*}(^1\Delta_g) + \mathrm{O^*}(^1\mathrm{D}), \tag{57}$$

$$\mathrm{O^*}(^1\mathrm{D}) + \mathrm{H_2O} \rightarrow \mathrm{OH} + \mathrm{OH}. \tag{58}$$

Quenching of excited O may occur to produce a ground state atom of O, but free ground state oxygen atoms will produce ozone (via reaction 40), allowing for recycling. If present, NO_2 derived from natural (primarily lightning) or anthropogenic (primarily fossil fuel combustion) sources can also undergo photolysis via

$$\mathrm{NO_2} \xrightarrow{h\nu} \mathrm{NO} + \mathrm{O}, \tag{59}$$

to provide a free oxygen atom for the production of tropospheric ozone and the formation of photochemical smog. Major outstanding questions about terrestrial atmospheric composition consider the abundance trends and formation and loss pathways of key reactive species, greenhouse gases, pollution sources, and aerosols; how chemical and physical processes in the troposphere and stratosphere will both shape and respond to changes in climate and atmospheric composition; and quantifying chemical transport and exchange between different planetary reservoirs, including the surface and interior.

4.3 Mars

Early estimates of Mars' atmospheric properties in the 18th and 19th centuries were provided by telescopic observations of shifting surface features, clouds, and atmospheric variability now attributed to dust storms. By the mid-20th century, ground-based spectroscopic observations had confirmed the existence of CO_2, and studies of Martian clouds and polar caps suggested $\sim$millibar surface pressures (e.g., Hess 1948; Kuiper 1952; Grandjean & Goody 1955; Kaplan *et al.* 1964). Improved constraints on composition (including the first confirmation of solid CO_2) and atmospheric pressure were provided by the *Mariner* missions (1964-1971), followed by the first *in-situ* measurements of the atmosphere by the *Viking 1* and *Viking 2* landers (1976). Since then, numerous lander, rover, and orbiter missions alongside ongoing ground-based observations have provided information about the composition and climate of Martian atmosphere, including missions specifically equipped to explore the climate history of Mars, such as the *Curiosity* rover (2012), the *Phoenix* lander (2008) and orbiters including *Mars Reconnaissance Orbiter* (2006), *Mangalyaan* (2014), *MAVEN* (2014), and the *ExoMars Trace Gas Orbiter* (2016).

The composition of the Martian atmosphere is summarized in Table 4. The thin and cold atmosphere of Mars consists primarily of CO_2 (95.3%) with small amounts of N_2 (2.7%) and Ar (1.6%), and a number of minor species produced from photochemical reactions. With an average surface temperature near 214 K and surface pressures near 6-10 millibar, Mars surface conditions are below the triple point for both H_2O (273.16 K, 6.1 mbar) and CO_2 (216.6 K, 5.2 bar) so that liquid water and liquid carbon dioxide are both unstable, even at equatorial or summer daytime highs near 300 K. Both CO_2 and H_2O can produce frost on the Martian surface and commonly form thin clouds over a wide range of altitudes (Pollack *et al.* 1977; Pearl *et al.* 2001; Clancy *et al.* 2003; Montmessin *et al.* 2006; Whiteway *et al.* 2009; Määttänen & F. 2021). Water ice also forms clouds above the polar regions during local fall and winter (the "polar hood"), and around Mars' high shield volcanoes (e.g., Leovy *et al.* 1973; Pollack *et al.* 1977; Benson *et al.* 2011).

Table 4: Composition of the Atmosphere of Mars

Gas	Abundance	Source	Sink
CO_2	95.32%	outgassing, sublimation	condensation
N_2	2.7%	outgassing	atmospheric escape
Ar	1.6%	outgassing	none
O_2	0.17%[a]	CO_2 photolysis	photoreduction
CO	0.08%	CO_2 photolysis	photooxidation
H_2O	0.03% (variable)	sublimation, desorption	condensation, adsorption
H_2	15 ppm[b]	H_2O photolysis	atmospheric escape
NO	∼100 ppm	photochemistry	photochemistry
Ne	2.5 ppm	outgassing	none
Kr	0.3 ppm	outgassing	none
Xe	0.08 ppm	outgassing	none
O_3	0.02-0.2 ppm	photochemistry	photochemistry
H_2O_2	23 ppb (variable)[c]	photochemistry	photodissociation
CH_4	0-7 ppb	unknown	photochemistry, unknown

Table adapted after Lodders & Fegley (1998), with updates from the literature where indicated. [a]Franz *et al.* (2017) *Curiosity* SAM instrument suite;[b]Krasnopolsky & Feldman (2001); [c]using mean column density from Encrenaz *et al.* (2004); [d]Webster *et al.* (2018) report a background level of 0.4 ppb based upon *Curiosity* Tunable Laser Spectroscopy measurements (see also Villanueva *et al.* 2013), whereas no CH_4 was detected by the ExoMars Trace Gas Orbiter (Korablev *et al.* 2019).

Despite the instability of liquid water at the surface of Mars today, starting with the apparent fluvial geomorpology revealed by *Mariner 9* (1971-1972), there is abundant geological and geochemical evidence that liquid water shaped Mars surface features in the distant past (e.g., Clifford 1993; Carr 1996; Bibring *et al.* 2006; Ehlmann *et al.* 2008, 2011). This has led to ongoing research exploring the conditions and mechanisms that could produce the observed surface features and mineralogy, and studies of the early climate history and evolution of the Martian atmosphere. These studies, along with observations of the upper atmosphere and exosphere, suggest extensive atmospheric loss that has transformed a warm and wet climate to the cold and dry planet we find today (Pollack *et al.* 1987; Jakosky & Phillips 2001; Jakosky *et al.* 2017, 2018). The water inventory on Mars is now mostly present as ice sequestered in the polar caps and the subsurface, and hydrated mineral deposits in the crust (e.g., Scheller *et al.* 2021; Wernicke & Jakosky 2021).

In the present-day atmosphere of Mars, large surface pressure variations are caused by the 25° tilt of Mars' axis which yields large temperature variations and the corresponding seasonal deposition and sublimation of significant amounts of CO_2 ice (and to a lesser extent H_2O ice) in the polar regions, summarized by the net reaction

$$CO_2(s) \rightleftarrows CO_2(g), \tag{60}$$

for which the equilibrium vapour pressure of CO_2 is $\sim$1 mbar at 140 K. Because CO_2 is the primary component of the atmosphere, this seasonal cycle provides significant interannual variability: surface pressures drop as more CO_2 is deposited into polar ice. For example, the *Viking* landers and *Curiosity* rover measured surface pressures ranging from 7 mbar to 10 mbar corresponding to seasonal behavior of the polar caps (Hess *et al.* 1977, 1980; Kelly *et al.* 2006; Trainer *et al.* 2019).

As on Venus, atmospheric CO_2 on Mars is also subject to loss via photolysis:

$$CO_2 \xrightarrow{h\nu} CO + O. \tag{61}$$

A key difference is that this photolysis can occur throughout the entire Martian atmospheric column down to the surface. Thus, Mars has the same stability problem as Venus, and CO_2 would be gradually removed from the atmosphere unless there is an efficient method for recycling production. Moreover, observations of CO (Kaplan *et al.* 1964) and O_2 (Barker 1972) show abundances lower than expected, suggesting a conversion mechanism back into CO_2 (e.g., see Nair *et al.* 1994).

The presence of atmospheric H_2O ($\sim$0.03%) allows for HO_x catalytic cycles that recycle CO_2. For example, McElroy & Donahue (1972) showed that CO_2 recombination can be catalyzed by OH radicals, which may produced by the the photolysis of H_2O via

$$H_2O \xrightarrow{h\nu} OH + H, \tag{62}$$

which can initiate a series of reactions:

$$\begin{aligned} OH + CO &\rightarrow CO_2 + H && (63)\\ H + O_2 &\xrightarrow{M} HO_2 && (64)\\ O + HO_2 &\rightarrow O_2 + OH && (65)\\ \hline CO + O &\rightarrow CO_2. && (66) \end{aligned}$$

The H atom produced by H_2O photolysis can also react with HO_2 to produce H_2 and O_2:

$$H + HO_2 \rightarrow H_2 + O_2. \tag{67}$$

The hydrogen produced in this way diffuses from the lower atmosphere to the upper atmosphere, where ionospheric reactions produce H atoms that are subject to thermal escape. This is supported by spectroscopic observations of H atoms in Mars' exosphere, and consistent with the escape of

H_2O in stoichiometric proportions (due to self-regulating photochemical processes; see Yung & DeMore 1999) over long periods of Martian history (Jakosky *et al.* 2015; Chaffin *et al.* 2017).

HO_x chemistry also plays a role in regulating the abundances of other key species such as ozone (O_3) and hydrogen peroxide (H_2O_2) in the Martian atmosphere (e.g., Nair *et al.* 1994; Lefèvre *et al.* 2008). As on Earth, ozone is produced by the sequence of reactions,

$$O_2 \xrightarrow{h\nu} 2O \tag{68}$$

$$O + O_2 \xrightarrow{M} O_3, \tag{69}$$

and is readily destroyed by H (a product of H_2O photolysis):

$$H + O_3 \rightarrow O_2 + OH. \tag{70}$$

This relationship yields an inverse correlation between the O_3 abundance and that of HO_x-producing water vapor, consistent with model-data comparisons and *Mars Express* observations of seasonal variations that show relatively high O_3 abundances during Mars' northern winter (Lefèvre *et al.* 2008). Hydrogen peroxide (H_2O_2), proposed as an oxidizing agent of the Martian regolith (Oyama & Berdahl 1977) and detected by microwave spectroscopy (Clancy *et al.* 2004; Encrenaz *et al.* 2004), is produced from HO_x via the reaction

$$HO_2 + HO_2 \rightarrow H_2O_2 + O_2. \tag{71}$$

The photolysis of H_2O_2 produces hydroxyl radicals

$$H_2O_2 \xrightarrow{h\nu} OH + OH. \tag{72}$$

The reactions above are expected to yield a positive correlation between the H_2O_2 abundance and that of water vapor. At high H_2O abundances, H_2O_2 photolysis is an important source of OH radicals in HO_x catalytic cycles beginning with reaction (63) that recycle CO and O back to CO_2.

The reported detections of trace and variable amounts of CH_4 by ground-based and *Mars Express* infrared spectroscopy and the *Curiosity* rover and the non-detection reported by the ExoMars Trace Gas Orbiter have been a subject of particular interest and debate (e.g., see Formisano *et al.* 2004; Mumma *et al.* 2009; Zahnle *et al.* 2011; Krasnopolsky 2012; Webster *et al.* 2013, 2015, 2018; Korablev *et al.* 2019). In the upper atmosphere ($>$ 70 km) CH_4 is readily destroyed by UV photolysis. In the lower atmosphere, CH_4 photolysis is shielded by UV absorption from CO_2, but is subject to oxidation (as on Earth) by OH radicals:

$$CH_4 + OH \rightarrow CH_3 + H_2O. \tag{73}$$

Taken together, these processes yield an CH_4 atmospheric lifetime of $\sim$300 years (e.g., Villanueva *et al.* 2013). Shorter period spatial and/or seasonal variations in the CH_4 abundance in Mars' atmosphere would thus rely upon atmospheric production and loss processes that remain poorly understood. A number of different methane sources have been proposed, including volcanism, microbial activity, or chemical reactions associated with metamorphism. This methane is plausibly destroyed by some yet-unidentified oxidizing agent such as H_2O_2. More generally, surface-atmosphere interactions and heterogeneous chemistry on ice or dust grains may play an important role in the oxidation of the Martian regolith and atmosphere. For example, model-data comparisons of Martian photochemistry suggest that hetereogenous chemistry is needed explain the relationship between observed gas abundances and photochemical model predictions (Anbar *et al.* 1993; Krasnopolsky 1993; Atreya & Gu 1994; Krasnopolsky 2006; Lefèvre *et al.* 2008). The results of the *Viking* lander biological experiments are also consistent with the presence of a strong oxidizing agent (Oyama & Berdahl 1977; Navarro-González *et al.* 2010; Encrenaz *et al.* 2012). The behavior of perchlorate (ClO_4^-) compounds, first detected at the *Phoenix* lander site (Hecht *et al.* 2009), may provide further clues. The redox chemistry of the Martian regolith and near-surface atmosphere (e.g., Spiga 2019) – and its relationship to the climate history of Mars – remains an subject of active observational, experimental, and theoretical investigation.

5 Giant planet atmospheres

The atmospheres of the gas giant planets exist as massive molecular envelopes consisting mostly of molecular hydrogen (H_2) and helium (He) captured as primary atmospheres from the solar nebula during planetary formation. In contrast to the terrestrial planets, the gas giants have no solid planetary surface. For this reason, their radii are defined adopting an atmospheric reference pressure of 1 bar (see Table 1), with pressures and temperatures increasing with depth into the troposphere. The atmospheric profiles for the gas giant planets down to the $\sim$20 bar level are shown in Figure 4.

The observed chemical abundances in the atmospheres of the giant planets are summarized in Table 5. To a rough first approximation, the giant planet atmospheres are protosolar in composition, with varying enhancements in heavy elements (i.e., elements heavier than He) such as carbon, nitrogen, and oxygen, present as hydrides. The low observed abundances of NH_3, H_2O, and H_2S on Saturn, Uranus, and Neptune are attributed to their sequestration into cloud layers a deeper atmospheric levels. In all four giant planets, the observed atmospheric chemistry is shaped by various chemical and physical processes including thermochemical equilibrium, reaction kinetics and atmospheric mixing, cloud formation, and photochemistry.

Table 5: Composition of Giant Planet Atmospheres

Gas	Protosolar^a	Jupiter	Saturn	Uranus	Neptune
Major species					
H_2	83.2%	86.4%	88%	$\sim$82.5%	$\sim$80%
He	16.6%	13.6%	11.9%^{d}	15.2%	19.0%
Condensible Species					
CH_4	602 ppm	2050 ppm^b	4500 ppm	2.3%	2-4%^{e}
NH_3	145 ppm	351 ppm^c	159 ppm	$<$ 100 ppb	$<$ 600 ppb
H_2O	882 ppm	2500 ppm^c	2-200 ppb	-	-
H_2S	29 ppm	77 ppm^b	$<$ 0.4 ppm	$<$ 0.8 ppm	$<$ 3 ppm
Deuterated Species					
HD		45 ppm	110 ppm	148 ppm	192 ppm
CH_3D		0.20 ppm	0.39 ppm	8.3 ppm	12 ppm
Noble Gases					
Ne	289 ppm	21 ppm	-	-	-
Ar	6.5 ppm	16 ppm	-	-	-
Kr	3.4 ppb	8 ppb	-	-	-
Xe	0.4 ppb	0.8 ppb	-	-	-
Disequilibrium and Photochemical Species					
PH_3	0.5 ppm	0.7 ppm	4.5 ppm	$<$ 1.1 ppb^f	-
GeH_4	7.9 ppb	0.7 ppb	0.4 ppb	-	-
AsH_3	0.4 ppb	0.22 ppb	2.1 ppb	-	-
CO		1 ppb	1.4 ppb	$<$ 40 ppb	0.65 ppm
CO_2		5-35 ppb	0.3 ppb	$<$ 0.3 ppb	$<$ 0.5 ppb
HCN		60 ppb	$<$ 4 ppb	$<$ 15 ppb	0.3 ppb
C_2H_2		0.11 ppm	0.30 ppm	10 ppb	60 ppb
C_2H_4		7 ppb	0.2 ppb	-	-
C_2H_6		5.8 ppm	7.0 ppm	10 ppb^g	1.5 ppm
C_4H_2		0.3 ppm	0.09 ppb	0.16 ppb^g	detected
CH_3C_2H		2.5 ppb	0.6 ppb	0.25 ppb^g	0.12 ppb

Abundances given as volume mixing ratios following the compilations of Lodders & Fegley (1998); Lodders & Fegley (2011) and de Pater & Lissauer (2015), with updates from the literature where indicated. ^{a}Estimated abundances in a protosolar-composition gas based upon the protosolar elemental abundances in Lodders (2020). The protosolar H_2O abundance is calculated assuming the prior removal of $\sim$20% of the oxygen inventory into rock-forming oxides. ^{b}Wong *et al.* (2004); ^{c}Li *et al.* (2020); ^{d}Conrath & Gautier (2000); ^{e}Irwin *et al.* (2019); ^{f}Teanby *et al.* (2019); ^{g}Burgdorf *et al.* (2006).

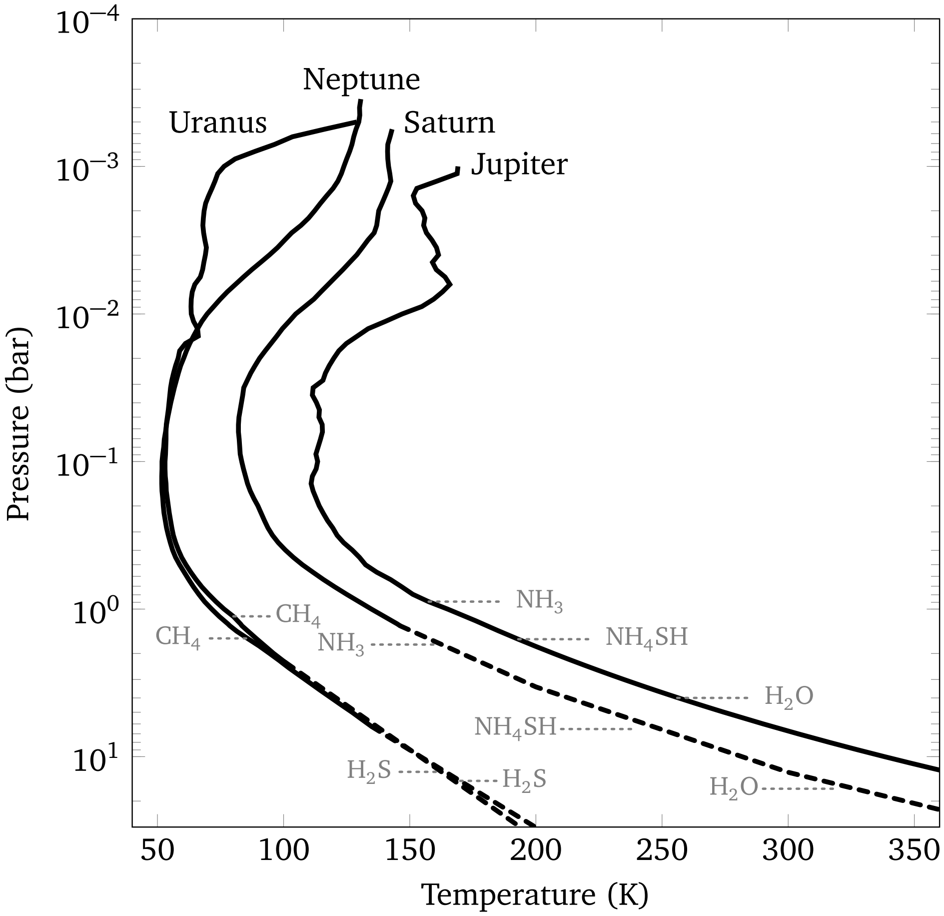

Figure 4: Atmospheric profiles for Jupiter, Saturn, Uranus, and Neptune, derived from *Voyager* radio occultation data (Lindal *et al.* 1985; Lindal 1992) and *in situ* observations of Jupiter's atmosphere by the *Galileo* entry probe (Seiff *et al.* 1998). The dashed lines are extensions of adiabatic profiles into the deep troposphere. The horizontal dotted lines denote the pressure and temperature of the cloud base (i.e., the greatest depth at which equilibrium condensation occurs) for different condensates (labeled) along each profile. For Uranus and Neptune, the NH_3, NH_4SH, and H_2O cloud layers are expected to condense at higher pressures and temperatures than shown here.

It is convenient to further divide the giant planets into two categories: the larger *gas giants* Jupiter and Saturn and the smaller *ice giants* Uranus and Neptune. The differences are most readily distinguished by a comparison of the inferred interior structures of the giant planets, as illustrated in Figure 5. Gas-rich Jupiter and Saturn are more massive (318 M_{E} and 95 M_{E}, respectively), larger (11.2 R_{E} and 9.5 R_{E}), and consist mostly of hydrogen and helium, with relatively small cores of rock and ice. Although Uranus (14.5 M_{E}, 4.0 R_{E}) and Neptune (17.1 M_{E}, 3.9 R_{E}) likewise possess hydrogen-rich molecular envelopes, these planets are significantly smaller and appear to contain a much greater proportion of "ice-forming" (e.g., C, N, O) and rocky (e.g., Mg, Si, Fe) elements. Here we will discuss the atmospheric chemistry of each of these sub-categories in turn, with a focus on tropospheric abundances and the processes shaping the observed compositions of giant planet atmospheres.

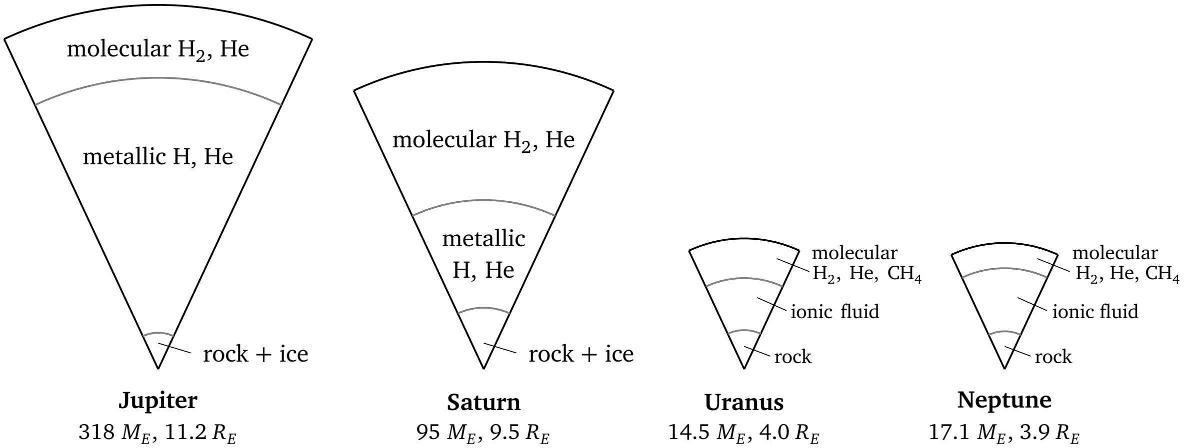

Figure 5: Simplified schematic cross-sections (drawn to scale) of the interior structures of Jupiter, Saturn, Uranus, and Neptune. See Stevenson (1982); Hubbard *et al.* (1995); Guillot (1999); Guillot *et al.* (2004); Marley & Fortney (2007) for details.

5.1 Jupiter and Saturn

The low densities of Jupiter (1.3 g cm^{-3}) and Saturn (0.7 g cm^{-3}), along with the presence of hydrides (e.g., CH_4, NH_3), led early observers and theorists to conclude that these giant planets consist mostly of hydrogen and have bulk compositions roughly similar to that of the Sun (e.g., Jeffreys 1924; Wildt 1932). Moreover, advances in our understanding of high-pressure materials, including the prediction of metallic hydrogen (Wigner & Huntington 1935) yielded early models of Jupiter and Saturn that consisted of H and He and included a metallic hydrogen layer (e.g., Brown 1950; Ramsey 1951; Demarcus 1958; Peebles 1964). High-pressure experiments and models, along with spacecraft measurements of the gravitational field have provided additional constraints for models of interior structure and composition. Jupiter and Saturn both appear to possess dense core of rock and possibly ice, an overlying mantle of fluid metallic hydrogen (stable at pressures above ∼2 Mbar), and an outer molecular H_2-He envelope (see Figure 5) of which only the uppermost portions are directly observable by remote-sensing or *in-situ* methods.

Far-infrared measurements show that both Jupiter and Saturn emit nearly twice as much energy than they receive from the Sun (Low 1966) suggestive of convecting interiors (Peebles 1964; Hubbard 1968, 1969). The composition of their visible atmospheres is thus expected to be generally representative of bulk atmospheric composition. For example, the tropospheric abundances of CH_4, NH_3, H_2S, and H_2O are generally assumed to represent the elemental abundances of the C, N, S, and the majority of planetary O (e.g., see Figure 6). However, recent *Juno* measurements of Jupiter's gravity field suggest the possibility of a diluted core and non-uniform heavy element mixing throughout the planet as a whole (e.g., Debras & Chabrier 2019; Wahl *et al.* 2017). The global distribution of heavy elements – and the extent to which tropospheric abundances are representative of a bulk planetary inventory – thus remain outstanding questions for observational and theoretical study.

Atmospheric abundances for Jupiter and Saturn are given in Table 5, derived mostly from ground- and spacecraft-based infrared observations (in particular, *Voyager 1-2*, *Galileo*, and *Juno* to Jupiter; *Voyager 1-2* and *Cassini* to Saturn). The *Galileo* entry probe also provided *in situ* mass spectrometer measurements of Jupiter's atmosphere down to 22-bar level, showing element-to-H_2 enrichments of $\sim 2-4\times$ relative to a protosolar composition for C, N, S, Ar, Kr, and Xe (Mahaffy *et al.* 2000; Wong *et al.* 2004) and depletions in others (Ne, He, and O; see Figure 6). However, the entry probe entered Jupiter's atmosphere in a "hot-spot" region characterized by low cloud opacity, low abundances of cloud-forming species, high thermal (5 μm) emission, and a water abundance that was still increasing with depth when the probe signal was lost. More recently, microwave observations (which probe as deep as ∼100 bar) by the *Juno* spacecraft suggest a deep H_2O abundance of 2500 ppm, corresponding to an oxygen enrichment roughly similar to that for other heavy elements (e.g., see Figure 6; Li *et al.* 2017; Li *et al.* 2020). On both planets, the depletion in He relative to a protosolar composition is attributed to the removal of He from the molecular envelope into the metallic H-He layer. A similar effect is observed for Ne on Jupiter, plausibly due to the incorporation of Ne into He droplets separating out of H-He metal (Roulston & Stevenson 1995; Fortney & Hubbard 2003).

A number of species condense in the upper tropospheres of both planets, producing (from the bottom up) an H_2O cloud consisting of aqueous solution and/or water ice, ammonium hydrosulfude (NH_4SH), and NH_3 ice (see Figure 4). Each cloud layer removes condensible species from the atmosphere and introduces cloud particles that contribute to opacity. For example, the bright zones of Jupiter's banded structure appear to be caused by icy NH_3 clouds. Removal by cloud formation also explains the low observed abundances of NH_3, H_2O, and H_2S in the stratosphere and upper troposphere Saturn, at altitudes above the condensation levels for each of these species. Abundance estimates from microwave observations predict higher abundances of NH_3, H_2O, and

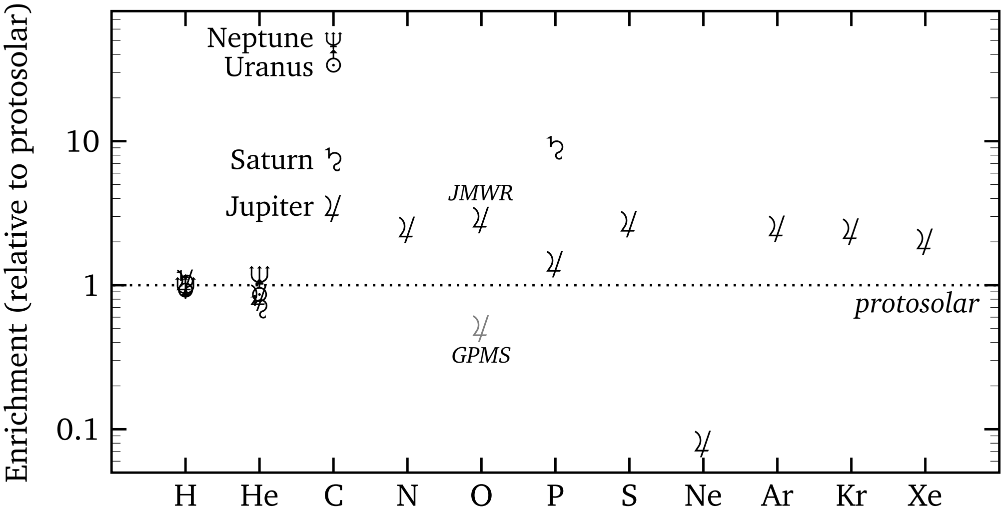

Figure 6: Observed element abundance inventories in the giant planets relative to a protosolar-composition gas (dotted line). Protosolar abundances are derived from Lodders (2020) assuming H as H_2, C as CH_4, N as NH_3, O as H_2O, P as PH_3, and S as H_2S. A limited number of elements are shown for Saturn (H, He, C, P), Uranus (H, He, C), and Neptune (H, He, C), as other species remain undetected or have been removed by condensation in the upper troposphere. For Jupiter, the H_2O abundance measured by the *Galileo* Probe Mass Spectrometer (GMPS) (Wong *et al.* 2004) and the *Juno* Microwave Radiometer (JMWR) (Li *et al.* 2017; Li *et al.* 2020) are shown for comparison.

H_2S at pressures between 5-10 bar, below their respective cloud layers (de Pater & Mitchell 1993). Heavy element abundances in Saturn's deep atmosphere are thus estimated from measurements of CH_4 and PH_3 (e.g., Visscher & Fegley 2005), which show element-to-H_2 enhancements of $\sim$7-9$\times$ relative to a protosolar composition.

The equilibrium condensate model was first developed to explain and identify tropospheric cloud formation of H_2O, NH_4SH, and NH_3 cloud layers on Jupiter and Saturn (Lewis 1969; Lewis & Prinn 1970; Weidenschilling & Lewis 1973; Atreya *et al.* 1996; Gierasch *et al.* 2000; Ingersoll *et al.* 2000). Additional cloud condensates (including, for example, Fe metal and Mg-silicates) are expected to form at higher pressures and temperatures in the deep atmospheres of both planets. This scenario is supported by several lines of evidence (e.g., see Lodders & Fegley 1994, 2006; Visscher *et al.* 2010a), including the detection of GeH_4 and absence of SiH_4 on Jupiter and Saturn (although $A_{\mathrm{Si}} > A_{\mathrm{Ge}}$), presumably due to the removal of Si into silicate clouds deeper in the amosphere, and by the detection of H_2S in Jupiter's atmosphere by the *Galileo* entry probe, which suggests removal of Fe into a deep cloud layer, as FeS formation would otherwise remove S from the gas phase above the $\sim$700 K level (because $A_{\mathrm{Fe}} > A_{\mathrm{Fe}}$; Fegley & Lodders 1994; Lodders & Fegley 2002; Visscher *et al.* 2006). Assuming uniform protosolar elemental abundance ratios (e.g., Si/O), the condensation of rock-forming elements in the deep atmosphere sequesters $\sim$ 20% of the total oxygen inventory in a protosolar-composition gas (Lodders 2004; Visscher & Fegley 2005; Visscher *et al.* 2010b; Lodders 2020), with the remainder mostly present as water vapour until H_2O

itself condenses in the upper troposphere.

A number of tropospheric species are present in abundances much greater than predicted by thermodynamic equilibrium. The two main disequilibrium processes in giant planet atmospheres are

- transport-induced quenching, which occurs when atmospheric mixing occurs faster than chemical reactions can act to maintain equilibrium, and
- photochemistry, which occurs when molecules are broken apart by stellar UV radiation that triggers subsequent chemical reactions.

The role of quench chemistry was first demonstrated for CO on Jupiter (Prinn & Barshay 1977). For species such as CO, PH_3, GeH_4, and AsH_3, observed abundances far in excess of thermodynamic predictions suggest rapid vertical mixing from warmer, deeper levels where each species has a greater abundance at an equilibrium maintained by fast reaction kinetics. However, departures from equilibrium occur at higher, cooler altitudes when vertical mixing occurs faster than chemical reactions can maintain equilibrium, effectively "quenching" the abundance of a molecular species at a fixed value throughout the upper troposphere (e.g., see Prinn & Barshay 1977; Fegley & Prinn 1985; Fegley & Lodders 1994; Visscher & Moses 2011; Wang *et al.* 2016; Visscher 2020). The behavior of these quenched species thus provides clues about the chemical composition down to $\sim$ kilobar levels in giant planet atmospheres (Giles *et al.* 2017a; Grassi *et al.* 2020; Visscher 2020).

Photochemistry also plays an important role in the stratosphere and upper troposphere of the gas giant planets. For example, short wavelength ultraviolet photons ($\lesssim$ 100 nm) are absorbed by H_2 photolysis in the upper stratosphere:

$$\mathrm{H_2} \xrightarrow{h\nu} \mathrm{2H}. \tag{74}$$

Methane is photolyzed (at $\sim 100-200$ nm) in the lower stratosphere via reactions such as

$$\mathrm{CH_4} \xrightarrow{h\nu} \mathrm{CH_3} + \mathrm{H}, \tag{75}$$

$$\mathrm{CH_4} \xrightarrow{h\nu} {}^1\mathrm{CH_2} + \mathrm{H_2}, \tag{76}$$

$$\mathrm{CH_4} \xrightarrow{h\nu} \mathrm{CH} + \mathrm{H_2} + \mathrm{H}. \tag{77}$$

The products of these photolysis reactions can then combine in various ways to produce heavier hydrocarbons including C_2H_2, C_2H_4, C_2H_6, C_4H_2, and CH_3C_2H, many of which have been observed in the upper atmospheres of the giant planets (e.g., see Gladstone *et al.* 1996; Moses *et al.*

2000, 2005). For example, key reactions for the production of C_2 species include

$$2CH_3 \xrightarrow{M} C_2H_6, \tag{78}$$

$$CH + CH_4 \rightarrow C_2H_4 + H, \tag{79}$$

$$2CH_2 \rightarrow C_2H_2 + H_2, \tag{80}$$

which can undergo additional photolysis and recombination reactions to produce higher hydrocarbons. The products of hydrocarbon photochemistry diffuse downward and are eventually recycled back into CH_4 at deeper, warmer levels in the atmosphere, so that there is no net loss of methane with time.

Most UV photons are absorbed by H_2 photolysis in the upper stratosphere and CH_4 photolysis in the lower stratosphere via the reactions above. However, longer wavelength UV photons ($>$ 150 nm) may penetrate into the upper troposphere to drive additional photochemical reactions involving NH_3, PH_3, and (to a lesser extent) H_2S:

$$NH_3 \xrightarrow{h\nu} NH_2 + H, \tag{81}$$

$$PH_3 \xrightarrow{h\nu} PH_2 + H, \tag{82}$$

$$H_2S \xrightarrow{h\nu} SH + H. \tag{83}$$

Each of these reactions produces H atoms and a reactive radical that leads to the formation of additional N, P, and S species, respectively, eventually producing condensates such as hydrazine (N_2H_4), red phosphorus (P_4; identified as a chromophore candidate for the Great Red Spot; Prinn & Lewis 1975), and elemental sulfur (S_8; a yellow chromophore candidate). Moreover, coupled NH_3-PH_3 photochemistry (and to a lesser extent CH_3-NH_3 chemistry that may produce the observed HCN) occurs because these gases absorb UV photons at similar atmospheric levels. Tropospheric photochemistry is thus a potential source of aerosols and chromophores in the upper atmospheres of Jupiter and Saturn (e.g., Atreya *et al.* 1977; Kaye & Strobel 1983, 1984; Edgington *et al.* 1998, 1999; West *et al.* 2007; Visscher *et al.* 2009), although the specific composition of chromospheric compound(s) remains unresolved.

5.2 Uranus and Neptune

Uranus (discovered in 1781 by Sir William Herschel) and Neptune (discovered in 1846 by Johann Galle, based upon the predictions of Urbain LeVerrier) are the only major planets in our Solar System not known from antiquity. Compared to Jupiter and Saturn (and lacking the extent of gravitational compression found on Jupiter), the relatively higher densities of Uranus (1.33 g cm^{-3}) and Neptune (1.64 g cm^{-3}) suggest a bulk composition with a greater proportion of heavy elements relative to H and He. Although CH_4 and molecular H_2 and a number of other planetary properties had been detected in both planets from ground-based observations in the early and mid-20th century (e.g., see Adel & Slipher 1934; Kuiper 1952; Herzberg 1952; Trafton 1981; Bergstralh 1984), our understanding of the atmospheric chemistry of Uranus and Neptune was greatly advanced by the *Voyager 2* flybys of Uranus in 1986 and of Neptune in 1989 (e.g., for reviews see Fegley *et al.* 1991; Gautier *et al.* 1995; Moses *et al.* 2020).

The observed atmospheric abundances for Uranus and Neptune are given in Table 5. Notably, radio occultation and infrared spectroscopic measurements by *Voyager 2* indicate He/H ratios on both planets that are roughly similar to the protosolar value (Conrath *et al.* 1987, 1991). This is higher than observed on Jupiter and Saturn, because Uranus and Neptune lack any H-He metallic layer (their interior pressures are too low) that could give rise to He differentiation. Instead, interior models of Uranus and Neptune generally include a core of rocky material, an overlying ionic/fluid mantle with abundant ice-forming elements (C, N, O), and an outer molecular H_2-He-CH_4 envelope (e.g., see Figure 5 and Stevenson 1982).

Large enrichments in heavy elements are likewise demonstrated by the high measured CH_4 abundance on each planet, which is 50-100$\times$ the CH_4/H_2 abundance ratio in a protosolar composition gas. The preferential absorption of red light by methane is responsible for the characteristic blue color of each planet. The atmospheres of Uranus and Neptune are also cold enough to yield CH_4 (and possibly H_2S) cloud formation in the upper troposphere, consistent with ground-based and *Voyager 2* observations of aerosols and hazes in atmospheres that are otherwise relatively clear over a large range of observable altitudes (e.g., Smith *et al.* 1989; Stone & Miner 1989; West *et al.* 1991; Baines *et al.* 1995). Enhancements for other heavy elements (N as NH_3, O as H_2O, etc) are anticipated but not observed, plausibly due to their removal into clouds and/or sequestration into an ionic fluid layer deeper in the atmosphere.

As for Jupiter and Saturn, stratospheric CH_4 photochemistry on Uranus and Neptune produces a number of hydrocarbon products including CH_3, C_2H_2, C_2H_4, C_2H_6, C_4H_2, and CH_3C_2H, several of which have been observed on both planets (e.g., see Table 5 and review in Moses *et al.* 2020). These products are also susceptible to ultraviolet photolysis and condensation, contributing to haze formation in the lower stratosphere (e.g., Romani & Atreya 1988; Summers & Strobel 1989; Moses *et al.* 1992, 1995). In the troposphere, longer-wavelength ultraviolet radiation is expected to efficiently photolyze PH_3 and may lead to the production of P_2H_4 (Teanby *et al.* 2019). However, coupled C-N or P-N photochemistry is not expected to play a significant role given the low upper-tropospheric abundance of NH_3.

Uranus displays a number of unique properties that are relevant for its atmospheric chemistry, including an obliquity of 97.9°between its rotation axis and orbital plane. Despite large variations in insolation over the course of a Uranian year, seasonal effects on hydrocarbon photochemistry are minimized due to poor mixing and long chemical lifetimes in the stratosphere (Moses *et al.*

2018). The internal heat flux from Uranus is also either very weak or nonexistent compared to the other giant planets, with a ratio of thermal radiation to absorbed solar energy of 1.06 ± 0.08 (Pearl *et al.* 1990). This heat source is plausibly explained by radiogenic heating from a $\sim 5M_{\mathrm{E}}$ rocky core of chondritic composition (Pearl *et al.* 1990; Podolak *et al.* 1991).

For comparison, Neptune emits $2.6\times$ more radiation than it receives from the Sun (2.61 ± 0.28; Conrath *et al.* 1991), which may drive more efficient tropospheric mixing than on Uranus. This behavior is consistent with differences the observed CO abundance on each planet: an upper limit of < 40 ppb on Uranus but as high as $\sim$1 ppm on Neptune. Although the detection of CO in the stratosphere suggests an external source of CO, tropospheric CO has generally been attributed to an internal source. As demonstrated by Lodders & Fegley (1994) the observed disequilibrium abundance of CO may thus provides estimates of the oxygen abundance (as H_2O) in the deep atmosphere, via the net thermochemical reaction

$$CH_4 + H_2O \rightleftarrows CO + 3H_2. \tag{84}$$

For a given CH_4 abundance, the quenched abundance of CO mixed into the upper troposphere depends CH_4-CO reaction kinetics, the rate of vertical mixing, and the deep H_2O abundance: more H_2O yields more CO. Following the conceptual approach of Prinn & Barshay (1977), chemical timescale and kinetics and transport modeling approaches yield constraints on the deep oxygen inventory of 250–650$\times$ protosolar on Neptune and an upper limit of $< 45 - 260\times$ protosolar on Uranus (e.g., Fegley & Prinn 1985, 1986; Lodders & Fegley 1994; Cavalié *et al.* 2017; Moses *et al.* 2020). Similar transport-induced quenching could also yield disequilibrium abundances of other carbon- and nitrogen-bearing species such as CO_2, N_2, and HCN (detected at 0.3 ppb on Neptune) in the upper atmospheres of both planets, which would provide better constraints on atmospheric mixing processes. Improved estimates of the CO tropospheric abundance on Uranus would allow for improved constraints on the deep water abundance and differences between the deep compositions of Uranus and Neptune, which – along with interior structures – remain poorly known. In general, the element abundance inventories of the giant planets appear to show increasing heavy element enrichment and increasing O/C abundance ratios moving outward in the solar system, suggestive of significant H_2O and heavy element enrichments on Uranus and Neptune. Such abundance trends thus may serve as a key constraint for models describing the formation and evolution of such “ice giant” planets both inside and outside our solar system.

For further reading

- Chamberlain, J. W. & Hunten, D. M., 1989. *Theory of Planetary Atmospheres: An Introduction to Their Physics and Chemistry.* Vol. 36 in International Geophysics Series. Academic Press.
- Yung, Y. L. & DeMore, W. B., 1999. *Photochemistry of Planetary Atmospheres*. New York: Oxford University Press
- Wayne, R., 2000. *Chemistry of Atmospheres: An Introduction to the Chemistry of the Atmospheres of Earth, the Planets, and Their Satellites*. Oxford University Press
- Lewis, J. 2004. *Physics and Chemistry of the Solar System, 2nd ed.* Vol. 87, International Geophysics Series. Academic Press.
- Lodders, K. & Fegley, B., Jr. 2011. *Chemistry of the Solar System.* Cambridge: Royal Society of Chemistry

References

Adams, W. S. and Dunham, J., T., 1932. Absorption Bands in the Infra-Red Spectrum of Venus. *Publications of the Astronomical Society of the Pacific*, 44, 243–245

Adel, A. and Slipher, V. M., 1934. Concerning the Carbon Dioxide Content of the Atmosphere of the Planet Venus. *Physical Review*, 46, 240–240

Alexander, C. M. O., Bowden, R., Fogel, M. L., Howard, K. T., Herd, C. D. K. and Nittler, L. R., 2012. The Provenances of Asteroids, and Their Contributions to the Volatile Inventories of the Terrestrial Planets. *Science*, 337, 721

Allen, D. A. and Crawford, J. W., 1984. Cloud structure on the dark side of Venus. *Nature*, 307, 222–224

Anbar, A. D., Leu, M. T., Nair, H. A. and Yung, Y. L., 1993. Adsorption of HO_x on aerosol surfaces: Implications for the atmosphere of Mars. *Journal of Geophysical Research*, 98, 10933–10940

Archer, D., Eby, M., Brovkin, V., Ridgwell, A., Cao, L., Mikolajewicz, U., Caldeira, K., Matsumoto, K., Munhoven, G., Montenegro, A. and Tokos, K., 2009. Atmospheric Lifetime of Fossil Fuel Carbon Dioxide. *Annual Review of Earth and Planetary Sciences*, 37, 117–134

Arney, G., Meadows, V., Crisp, D., Schmidt, S. J., Bailey, J. and Robinson, T., 2014. Spatially resolved measurements of H_2O, HCl, CO, OCS, SO_2, cloud opacity, and acid concentration in the Venus near-infrared spectral windows. *Journal of Geophysical Research (Planets)*, 119, 1860–1891

Atreya, S., Owen, T. and Wong, M., 1996. Condensible volatiles, clouds, and implications for meteorology in the *Galileo* probe entry region: Jupiter is not dry! *Bulletin of the American Astronomical Society*, 28, 1133

Atreya, S. K., Donahue, T. M. and Kuhn, W. R., 1977. The distribution of ammonia and its photochemical products on Jupiter. *Icarus*, 31, 348–355

Atreya, S. K. and Gu, Z. G., 1994. Stability of the Martian atmosphere: Is heterogeneous catalysis essential? *Journal of Geophysical Research*, 99, 13133–13146

Atreya, S. K., Pollack, J. B. and Matthews, M. S., 1989. *Origin and Evolution of Planetary and Satellite Atmospheres*. University of Arionza Press, Tucson

Avice, G. and Marty, B., 2020. Perspectives on Atmospheric Evolution from Noble Gas and Nitrogen Isotopes on Earth, Mars & Venus. *Space Science Reviews*, 216, 36. `2003.11431`

Baines, K. H., Hammel, H. B., Rages, K. A., Romani, P. N. and Samuelson, R. E., 1995. *Clouds and hazes in the atmosphere of Neptune.* 489–546

Barath, F. T., Barrett, A. H., Copeland, J., Jones, D. E. and Lilley, A. E., 1964. Symposium on Radar and Radiometric Observations of Venus during the 1962 Conjunction: Mariner 2 microwave radiometer experiment and results. *Astronomical Journal*, 69, 49

Barker, E. S., 1972. Detection of Molecular Oxygen in the Martian Atmosphere. *Nature*, 238, 447–448

Barker, E. S., 1979. Detection of SO_2 in the UV spectrum of Venus. *Geophysical Research Letters*, 6, 117–120

Bates, D. R. and Nicolet, M., 1950. The Photochemistry of Atmospheric Water Vapor. *Journal of Geophysical Research*, 55, 301–327

Baum, W. A. and Code, A. D., 1953. A photometric observation of the occultation of σ ARIETIS by Jupiter. *Astronomical Journal*, 58, 108–112

Benson, J. L., Kass, D. M. and Kleinböhl, A., 2011. Mars' north polar hood as observed by the Mars Climate Sounder. *Journal of Geophysical Research (Planets)*, 116, E03008

Bergstralh, J. T., 1984. Uranus and neptune. *NASA Conference Publication 2330*

Bézard, B. and de Bergh, C., 2007. Composition of the atmosphere of Venus below the clouds. *Journal of Geophysical Research (Planets)*, 112, E04S07

Bibring, J.-P. et al, 2006. Global Mineralogical and Aqueous Mars History Derived from OMEGA/Mars Express Data. *Science*, 312, 400–404

Bierson, C. J. and Zhang, X., 2020. Chemical Cycling in the Venusian Atmosphere: A Full Photochemical Model From the Surface to 110 km. *Journal of Geophysical Research (Planets)*, 125, e06159

Brown, H., 1950. On the Compositions and Structures of the Planets. *Astrophysical Journal*, 111, 641

Burgdorf, M., Orton, G., van Cleve, J., Meadows, V. and Houck, J., 2006. Detection of new hydrocarbons in Uranus' atmosphere by infrared spectroscopy. *Icarus*, 184, 634–637

Burton, M. R., Sawyer, G. M. and Granieri, D., 2013. Deep Carbon Emissions from Volcanoes. *Reviews in Mineralogy and Geochemistry*, 75, 323–354

Caldeira, K. and Wickett, M. E., 2003. Oceanography: Anthropogenic carbon and ocean ph

Carr, M. H., 1996. *Water on Mars*. Oxford University Press, New York

Catling, D. C. and Claire, M. W., 2005. How earth's atmosphere evolved to an oxic state: A status report. *Earth and Planetary Science Letters*, 237, 1–20

Cavalié, T., Venot, O., Selsis, F., Hersant, F., Hartogh, P. and Leconte, J., 2017. Thermochemistry and vertical mixing in the tropospheres of Uranus and Neptune: How convection inhibition can affect the derivation of deep oxygen abundances. *Icarus*, 291, 1–16. `1703.04358`

Chaffin, M. S., Deighan, J., Schneider, N. M. and Stewart, A. I. F., 2017. Elevated atmospheric escape of atomic hydrogen from Mars induced by high-altitude water. *Nature Geoscience*, 10, 174–178

Chamberlain, J. W. and Hunten, D. M., 1989. *Theory of Planetary Atmospheres : An Introduction to Their Physics and Chemistry.* Number Vol. 36 in International Geophysics. Academic Press

Chambers, J. E., 2014. *Planet Formation*, volume 2. 55–72

Chapman, S., 1930. A theory of upper-atmosphere ozone. *Memoirs of the Royal Meterological Society*, 3, 103–110

Clancy, R. T., Sandor, B. J. and Moriarty-Schieven, G. H., 2004. A measurement of the 362 GHz absorption line of Mars atmospheric H_2O_2. *Icarus*, 168, 116–121

Clancy, R. T., Wolff, M. J. and Christensen, P. R., 2003. Mars aerosol studies with the MGS TES emission phase function observations: Optical depths, particle sizes, and ice cloud types versus latitude and solar longitude. *Journal of Geophysical Research (Planets)*, 108, 5098

Clifford, S. M., 1993. A model for the hydrologic and climatic behavior of water on Mars. *Journal of Geophysical Research*, 98, 10973–11016

Connes, P., Connes, J., Benedict, W. S. and Kaplan, L. D., 1967. Traces of HCl and HF in the atmosphere of Venus. *Astrophysical Journal*, 147, 1230–1237

Conrath, B., Gautier, D., Hanel, R., Lindal, G. and Marten, A., 1987. The helium abundance of Uranus from Voyager measurements. *Journal of Geophysical Research*, 92, 15003–15010

Conrath, B. J. and Gautier, D., 2000. Saturn helium abundance: A reanalysis of *Voyager* measurements. *Icarus*, 144, 124–134

Conrath, B. J., Gautier, D., Lindal, G. F., Samuelson, R. E. and Shaffer, W. A., 1991. The helium abundance of Neptune from Voyager measurements. *Journal of Geophysical Research*, 96, 18907–18919

Conway, R. R., McCoy, R. P., Barth, C. A. and Lane, A. L., 1979. Iue detection of sulfur dioxide in the atmosphere of Venus. *Geophysical Research Letters*, 6, 629–631

Dauphas, N., Robert, F. and Marty, B., 2000. The Late Asteroidal and Cometary Bombardment of Earth as Recorded in Water Deuterium to Protium Ratio. *Icarus*, 148, 508–512

de Pater, I. and Lissauer, J. J., 2015. *Planetary Sciences*. Cambridge University Press, 2nd edition

de Pater, I. and Mitchell, D. L., 1993. Radio Observations of the planets: The importance of laboratory measurements. *Journal of Geophysical Research*, 98, 5471–5490

Debras, F. and Chabrier, G., 2019. New Models of Jupiter in the Context of Juno and Galileo. *Astrophysical Journal*, 872, 100. `1901.05697`

Demarcus, W. C., 1958. The constitution of Jupiter and Saturn. *Astronomical Journal*, 63, 2

Dobson, G. M. B. and Harrison, D. N., 1926. Measurements of the Amount of Ozone in the Earth's Atmosphere and Its Relation to Other Geophysical Conditions. *Proceedings of the Royal Society of London Series A*, 110, 660–693

Domingue, D. L., Koehn, P. L., Killen, R. M., Sprague, A. L., Sarantos, M., Cheng, A. F., Bradley, E. T. and McClintock, W. E., 2007. Mercury's Atmosphere: A Surface-Bounded Exosphere. *Space Science Reviews*, 131, 161–186

Draper, H., 1877. Photographs of the Spectra of Venus and α Lyrae. *Memorie della Societa Degli Spettroscopisti Italiani*, 6, A2–A9

Draper, H., 1879. On photographing the spectra of the stars and planets. *Memorie della Societa Degli Spettroscopisti Italiani*, 8, A81–A86

Duncan, M. S. and Dasgupta, R., 2017. Rise of Earth's atmospheric oxygen controlled by efficient subduction of organic carbon. *Nature Geoscience*, 10, 387–392

Dunham, J., Theodore, 1949. Spectroscopic Observations of the Planets at Mount Wilson. In *The Atmospheres of the Earth and Planets* (G. P. Kuiper, ed.). 288

Edgington, S. G., Atreya, S. K., Trafton, L. M., Caldwell, J. J., Beebe, R. F., Simon, A. A. and West, R. A., 1999. Ammonia and Eddy Mixing Variations in the Upper Troposphere of Jupiter from HST Faint Object Spectrograph Observations. *Icarus*, 142, 342–356

Edgington, S. G., Atreya, S. K., Trafton, L. M., Caldwell, J. J., Beebe, R. F., Simon, A. A., West, R. A. and Barnet, C., 1998. On the Latitude Variation of Ammonia, Acetylene, and Phosphine Altitude Profiles on Jupiter from HST Faint Object Spectrograph Observations. *Icarus*, 133, 192–209

Ehlmann, B. L., Mustard, J. F., Murchie, S. L., Bibring, J.-P., Meunier, A., Fraeman, A. A. and Langevin, Y., 2011. Subsurface water and clay mineral formation during the early history of Mars. *Nature*, 479, 53–60

Ehlmann, B. L., Mustard, J. F., Murchie, S. L., Poulet, F., Bishop, J. L., Brown, A. J., Calvin, W. M., Clark, R. N., Des Marais, D. J., Milliken, R. E., Roach, L. H., Roush, T. L., Swayze, G. A. and Wray, J. J., 2008. Orbital Identification of Carbonate-Bearing Rocks on Mars. *Science*, 322, 1828

Elliot, J. L., Hammel, H. B., Wasserman, L. H., Franz, O. G., McDonald, S. W., Person, M. J., Olkin, C. B., Dunham, E. W., Spencer, J. R., Stansberry, J. A., Buie, M. W., Pasachoff, J. M., Babcock, B. A. and McConnochie, T. H., 1998. Global warming on Triton. *Nature*, 393, 765–767

Encrenaz, T., Bézard, B., Greathouse, T. K., Richter, M. J., Lacy, J. H., Atreya, S. K., Wong, A. S., Lebonnois, S., Lefèvre, F. and Forget, F., 2004. Hydrogen peroxide on Mars: evidence for spatial and seasonal variations. *Icarus*, 170, 424–429

Encrenaz, T., Greathouse, T. K., Lefèvre, F. and Atreya, S. K., 2012. Hydrogen peroxide on Mars: Observations, interpretation and future plans. *Planetary & Space Science*, 68, 3–17

Fabry, C., 1929. Le rôle des Atmosphères dans les Occultations par les Planètes. *Journal des Observateurs*, 12, 1

Fegley, B., 1997. NOTE: Why Pyrite Is Unstable on the Surface of Venus. *Icarus*, 128, 474–479

Fegley, B., Zolotov, M. Y. and Lodders, K., 1997. The Oxidation State of the Lower Atmosphere and Surface of Venus. *Icarus*, 125, 416–439

Fegley, B., Jr., 2014. Venus. In *Meteorites, Comets, and Planets* (J. Farquhar, D. Canfield, & J. Kasting, eds.), Treatise on Geochemistry, (H. D. Holland and K. K. Turekian, eds.). Elsevier Science, 2nd edition

Fegley, B., Jr., Gautier, D., Owen, T. and Prinn, R. G., 1991. Spectroscopy and chemistry of the atmosphere of Uranus. In *Uranus* (J. T. Bergstralh, E. D. Miner, & M. S. Matthews, eds.). Tuscon: Univ. of Arizona Press, 147–203

Fegley, B., Jr. and Lodders, K., 1994. Chemical models of the deep atmospheres of Jupiter and Saturn. *Icarus*, 110, 117–154

Fegley, B., Jr. and Prinn, R. G., 1985. Equilibrium and nonequilibrium chemistry of Saturn's atmosphere - Implications for the observability of PH_3, N_2, CO, and GeH_4. *Astrophysical Journal*, 299, 1067–1078

Fegley, B., Jr. and Prinn, R. G., 1986. Chemical models of the deep atmosphere of Uranus. *Astrophysical Journal*, 307, 852–865

Fegley, B., Jr. and Prinn, R. G., 1989. *The Formation and Evolution of Planetary Systems*. Cambridge: Cambridge Univ. Press, 171–211

Formisano, V., Atreya, S., Encrenaz, T., Ignatiev, N. and Giuranna, M., 2004. Detection of Methane in the Atmosphere of Mars. *Science*, 306, 1758–1761

Fortney, J. J. and Hubbard, W. B., 2003. Phase separation in giant planets: inhomogeneous evolution of Saturn. *Icarus*, 164, 228–243

Fowler, A. and Strutt, R. J., 1917. Absorption Bands of Atmospheric Ozone in the Spectra of Sun and Stars. *Proceedings of the Royal Society of London Series A*, 93, 577–586

Franz, H. B., Trainer, M. G., Malespin, C. A., Mahaffy, P. R., Atreya, S. K., Becker, R. H., Benna, M., Conrad, P. G., Eigenbrode, J. L., Freissinet, C., Manning, H. L. K., Prats, B. D., Raaen, E. and Wong, M. H., 2017. Initial SAM calibration gas experiments on Mars: Quadrupole mass spectrometer results and implications. *Planetary & Space Science*, 138, 44–54

Frederick, J. E., 2008. *Principles of Atmospheric Science*. Reading, Massachusetts: Jones & Bartlett Learning

Friedlingstein, P., O'Sullivan, M., Jones, M. W. et al, 2020. Global Carbon Budget 2020. *Earth System Science Data*, 12, 3269–3340

Galloway, J. N., Leach, A. M., Bleeker, A. and Erisman, J. W., 2013. A chronology of human understanding of the nitrogen cycle. *Philosophical Transactions of the Royal Society B: Biological Sciences*, 368, 20130120

Gautier, D., Conrath, B. J., Owen, T., de Pater, I. and Atreya, S. K., 1995. The troposphere of Neptune. In *Neptune and Triton*. 547–611

Gierasch, P. J., Ingersoll, A. P., Banfield, D., Ewald, S. P., Helfenstein, P., Simon-Miller, A., Vasavada, A., Breneman, H. H., Senske, D. A. and A4 Galileo Imaging Team, 2000. Observation of moist convection in Jupiter's atmosphere. *Nature*, 403, 628–630

Giles, R. S., Fletcher, L. N. and Irwin, P. G. J., 2017a. Latitudinal variability in Jupiter's tropospheric disequilibrium species: GeH_4, AsH_3 and PH_3. *Icarus*, 289, 254–269. `1610.09073`

Gladstone, G. R., Allen, M. and Yung, Y. L., 1996. Hydrocarbon photochemistry in the upper atmosphere of Jupiter. *Icarus*, 119, 1–52

Grandjean, J. and Goody, R. M., 1955. The Concentration of Carbon Dioxide in the Atmosphere of Mars. *Astrophysical Journal*, 121, 548

Grassi, D., Adriani, A., Mura, A., Atreya, S. K., Fletcher, L. N., Lunine, J. I., Orton, G. S., Bolton, S., Plainaki, C., Sindoni, G., Altieri, F., Cicchetti, A., Dinelli, B. M., Filacchione, G., Migliorini, A., Moriconi, M. L., Noschese, R., Olivieri, A., Piccioni, G., Sordini, R., Stefani, S., Tosi, F. and Turrini, D., 2020. On the Spatial Distribution of Minor Species in Jupiter's Troposphere as Inferred From Juno JIRAM Data. *Journal of Geophysical Research (Planets)*, 125, e06206

Guillot, T., 1999. Interior of giant planets inside and outside the solar system. *Science*, 286, 72–77

Guillot, T., Stevenson, D. J., Hubbard, W. B. and Saumon, D., 2004. The interior of Jupiter. In *Jupiter. The Planet, Satellites and Magnetosphere* (F. Bagenal, T. E. Dowling, & W. B. McKinnon, eds.). Cambridge: Cambridge Univ. Press, 35–57

Halliday, A. N., 2013. The origins of volatiles in the terrestrial planets. *Geochimica et Cosmochimica Acta*, 105, 146–171

Hartley, W. N., 1881. Xxi. on the absorption of solar rays by atmospheric ozone. *J Chem Soc, Trans*, 39, 111–128

Hecht, M. H., Kounaves, S. P., Quinn, R. C., West, S. J., Young, S. M. M., Ming, D. W., Catling, D. C., Clark, B. C., Boynton, W. V., Hoffman, J., DeFlores, L. P., Gospodinova, K., Kapit, J. and Smith, P. H., 2009. Detection of Perchlorate and the Soluble Chemistry of Martian Soil at the Phoenix Lander Site. *Science*, 325, 64

Herschel, W., 1784. On the Remarkable Appearances at the Polar Regions of the Planet Mars, the Inclination of Its Axis, the Position of Its Poles, and Its Spheroidical Figure; With a Few Hints Relating to Its Real Diameter and Atmosphere. By William Herschel, Esq. F. R. S. *Philosophical Transactions of the Royal Society of London Series I*, 74, 233–273

Herzberg, G., 1952. Spectroscopic evidence of molecular hydrogen in the atmospheres of Uranus and Neptune. *Astrophysical Journal*, 115, 337–340

Hess, S. L., 1948. A Meteorological Approach to the Question of Water Vapor on Mars and the Mass of the Martian Atmosphere. *Publications of the Astronomical Society of the Pacific*, 60, 289

Hess, S. L., Henry, R. M., Leovy, C. B., Ryan, J. A. and Tillman, J. E., 1977. Meteorological results from the surface of Mars: Viking 1 and 2. *Journal of Geophysical Research*, 82, 4559–4574

Hess, S. L., Ryan, J. A., Tillman, J. E., Henry, R. M. and Leovy, C. B., 1980. The annual cycle of pressure on Mars measured by Viking Landers 1 and 2. *Geophysical Research Letters*, 7, 197–200

Holstein-Rathlou, C., Maue, A. and Withers, P., 2016. Atmospheric studies from the Mars Science Laboratory Entry, Descent and Landing atmospheric structure reconstruction. *Planetary & Space Science*, 120, 15–23

Hörst, S. M., 2017. Titan's atmosphere and climate. *Journal of Geophysical Research (Planets)*, 122, 432–482. `1702.08611`

Hubbard, W. B., 1968. Thermal structure of Jupiter. *Astrophysical Journal*, 152, 745–754

Hubbard, W. B., 1969. Thermal models of Jupiter and Saturn. *Astrophysical Journal*, 155, 333–+

Hubbard, W. B., Podolak, M. and Stevenson, D. J., 1995. The interior of Neptune. In *Neptune and Triton*. 109–138

Huggins, W., 1867. On the Spectrum of Mars, with some Remarks on the Colour of that Planet. *Monthly Notices of the Royal Astronomical Society*, 27, 178

Huggins, W., 1876. Note on the Photographic Spectra of Stars. *Proceedings of the Royal Society of London Series I*, 25, 445–446

Ingersoll, A. P., Gierasch, P. J., Banfield, D., Vasavada, A. R. and A3 *Galileo* Imaging Team, 2000. Moist convection as an energy source for the large-scale motions in Jupiter's atmosphere. *Nature*, 403, 630–632

Irwin, P. G. J., Toledo, D., Braude, A. S., Bacon, R., Weilbacher, P. M., Teanby, N. A., Fletcher, L. N. and Orton, G. S., 2019. Latitudinal variation in the abundance of methane (CH_4) above the clouds in Neptune's atmosphere from VLT/MUSE Narrow Field Mode Observations. *Icarus*, 331, 69–82. `1905.03516`

Jakosky, B. M. and Phillips, R. J., 2001. Mars' volatile and climate history. *Nature*, 412, 237–244

Jakosky, B. M., Slipski, M., Benna, M., Mahaffy, P., Elrod, M., Yelle, R., Stone, S. and Alsaeed, N., 2017. Mars' atmospheric history derived from upper-atmosphere measurements of ^{38}Ar/^{36}Ar. *Science*, 355, 1408–1410

Jakosky, B. M. et al, 2015. The Mars Atmosphere and Volatile Evolution (MAVEN) Mission. *Space Science Reviews*, 195, 3–48

Jakosky, B. M. et al, 2018. Loss of the Martian atmosphere to space: Present-day loss rates determined from MAVEN observations and integrated loss through time. *Icarus*, 315, 146–157

Jeffreys, H., 1924. On the internal constitution of Jupiter and Saturn. *Monthly Notices of the Royal Astronomical Society*, 84, 534

Johnson, B. and Goldblatt, C., 2015. The nitrogen budget of earth. *Earth-Science Reviews*, 148, 150–173

Kaplan, L. D., Münch, G. and Spinrad, H., 1964. An Analysis of the Spectrum of Mars. *Astrophysical Journal*, 139, 1

Kaye, J. A. and Strobel, D. F., 1983. Phosphine photochemistry in Saturn's atmosphere. *Geophysical Research Letters*, 10, 957–960

Kaye, J. A. and Strobel, D. F., 1984. Phosphine photochemistry in the atmosphere of Saturn. *Icarus*, 59, 314–335

Keeling, R. F. and Keeling, C., 2017. Atmospheric Monthly In Situ CO2 Data - Mauna Loa Observatory, Hawaii. In *Scripps CO2 Program Data, UC San Diego Library Digital Collections.*

Kelly, N. J., Boynton, W. V., Kerry, K., Hamara, D., Janes, D., Reedy, R. C., Kim, K. J. and Haberle, R. M., 2006. Seasonal polar carbon dioxide frost on Mars: CO_2 mass and columnar thickness distribution. *Journal of Geophysical Research (Planets)*, 111, E03S07

Killen, R., Cremonese, G., Lammer, H., Orsini, S., Potter, A. E., Sprague, A. L., Wurz, P., Khodachenko, M. L., Lichtenegger, H. I. M., Milillo, A. and Mura, A., 2007. Processes that Promote and Deplete the Exosphere of Mercury. *Space Science Reviews*, 132, 433–509

Killen, R. M. and Ip, W.-H., 1999. The surface-bounded atmospheres of Mercury and the Moon. *Reviews of Geophysics*, 37, 361–406

Kirchhoff, G., 1860. Ueber das Verhältniss zwischen dem Emissionsvermögen und dem Absorptionsvermögen der Körper für Wärme und Licht. *Annalen der Physik*, 185, 275–301

Kirchhoff, G. and Bunsen, R., 1860. Chemische Analyse durch Spectralbeobachtungen. *Annalen der Physik*, 186, 161–189

Kolodner, M. A. and Steffes, P. G., 1998. The Microwave Absorption and Abundance of Sulfuric Acid Vapor in the Venus Atmosphere Based on New Laboratory Measurements. *Icarus*, 132, 151–169

Korablev, O., Avandaele, A. C., Montmessin, F. et al, 2019. No detection of methane on Mars from early ExoMars Trace Gas Orbiter observations. *Nature*, 568, 517–520

Krasnopolsky, V. A., 1993. Photochemistry of the Martian Atmosphere (Mean Conditions). *Icarus*, 101, 313–332

Krasnopolsky, V. A., 2006. Photochemistry of the martian atmosphere: Seasonal, latitudinal, and diurnal variations. *Icarus*, 185, 153–170

Krasnopolsky, V. A., 2012. A photochemical model for the Venus atmosphere at 47-112 km. *Icarus*, 218, 230–246

Krasnopolsky, V. A. and Feldman, P. D., 2001. Detection of Molecular Hydrogen in theAtmosphere of Mars. *Science*, 294, 1914–1917

Kuiper, G. P., 1952. *The atmospheres of the earth and planets.* University of Chicago Press, revised edition

Lammer, H., Brasser, R., Johansen, A., Scherf, M. and Leitzinger, M., 2021. Formation of Venus, Earth and Mars: Constrained by Isotopes. *Space Science Reviews*, 217, 7. `2102.06173`

Lary, D. J., 1997. Catalytic destruction of stratospheric ozone. *Journal of Geophysical Research*, 102, 21,515–21,526

Lefèvre, F., Bertaux, J.-L., Clancy, R. T., Encrenaz, T., Fast, K., Forget, F., Lebonnois, S., Montmessin, F. and Perrier, S., 2008. Heterogeneous chemistry in the atmosphere of Mars. *Nature*, 454, 971–975

Lellouch, E., 2005. Io's Atmosphere and Surface-Atmosphere Interactions. *Space Science Reviews*, 116, 211–224

Lellouch, E., de Bergh, C., Sicardy, B., Ferron, S. and Käufl, H. U., 2010. Detection of CO in Triton's atmosphere and the nature of surface-atmosphere interactions. *Astronomy & Astrophysics*, 512, L8. `1003.2866`

Leovy, C. B., Briggs, G. A. and Smith, B. A., 1973. Mars Atmosphere during the Mariner 9 Extended Mission: Television Results. *Journal of Geophysical Research*, 78, 4252–4266

Lewis, J. S., 1969. The clouds of Jupiter and the NH_3-H_2O and NH_3-H_2S systems. *Icarus*, 10, 365–378

Lewis, J. S. and Prinn, R. G., 1970. Jupiter's clouds: structure and composition. *Science*, 169, 472–473

Li, C., Ingersoll, A., Bolton, S., Levin, S., Janssen, M., Atreya, S., Lunine, J., Steffes, P., Brown, S., Guillot, T., Allison, M., Arballo, J., Bellotti, A., Adumitroaie, V., Gulkis, S., Hodges, A., Li, L., Misra, S., Orton, G., Oyafuso, F., Santos-Costa, D., Waite, H. and Zhang, Z., 2020. The water abundance in jupiter's equatorial zone. *Nature Astron*

Li, C., Ingersoll, A., Janssen, M., Levin, S., Bolton, S., Adumitroaie, V., Allison, M., Arballo, J., Bellotti, A., Brown, S., Ewald, S., Jewell, L., Misra, S., Orton, G., Oyafuso, F., Steffes, P. and Williamson, R., 2017. The distribution of ammonia on Jupiter from a preliminary inversion of Juno microwave radiometer data. *Geophysical Research Letters*, 44, 5317–5325

Lilley, A. E., 1961. The Temperature of Venus. *Astronomical Journal*, 70, 290

Limaye, S. S., Grassi, D., Mahieux, A., Migliorini, A., Tellmann, S. and Titov, D., 2018. Venus Atmospheric Thermal Structure and Radiative Balance. *Space Science Reviews*, 214, 102

Lindal, G. F., 1992. The atmosphere of Neptune - an analysis of radio occultation data acquired with Voyager 2. *Astronomical Journal*, 103, 967–982

Lindal, G. F., Sweetnam, D. N. and Eshleman, V. R., 1985. The atmosphere of Saturn - an analysis of the *Voyager* radio occultation measurements. *Astronomical Journal*, 90, 1136–1146

Lissauer, J. J., 1993. Planet formation. *Annual Review of Astronomy & Astrophysics*, 31, 129–174

Lodders, K., 2004. Jupiter formed with more tar than ice. *Astrophysical Journal*, 611, 587–597

Lodders, K., 2020. Solar Elemental Abundances. *Oxford Research Encyclopedia of Planetary Science*

Lodders, K. and Fegley, B., 2011. *Chemistry of the Solar System.* Cambridge: Royal Society of Chemistry

Lodders, K. and Fegley, B., Jr., 1994. The origin of carbon monoxide in Neptunes's atmosphere. *Icarus*, 112, 368–375

Lodders, K. and Fegley, B., Jr., 1998. *The Planetary Scientist's Companion*. New York: Oxford Univ. Press

Lodders, K. and Fegley, B., Jr., 2002. Atmospheric chemistry in giant planets, brown dwarfs, and low-mass dwarf stars. I. Carbon, nitrogen, and oxygen. *Icarus*, 155, 393–424

Lodders, K. and Fegley, B., Jr., 2006. Chemistry of Low Mass Substellar Objects. In *Astrophysics Update 2* (J. W. Mason, ed.). Berlin: Springer Verlag, 1–28

Low, F. J., 1966. Observations of Venus, Jupiter, and Saturn at $\lambda 20\mu$. *Astronomical Journal*, 71, 391–+

Lunine, J. I., Coradini, A., Gautier, D., Owen, T. C. and Wuchterl, G., 2004. The origin of Jupiter. In *Jupiter. The Planet, Satellites and Magnetosphere* (F. Bagenal, T. E. Dowling, & W. B. McKinnon, eds.). Cambridge: Cambridge Univ. Press, 19–34

Lyons, T. W., Reinhard, C. T. and Planavsky, N. J., 2014. The rise of oxygen in Earth's early ocean and atmosphere. *Nature*, 506, 307–315

Määttänen, A. and F., M., 2021. Clouds in the Martian Atmosphere. *Oxford Research Encyclopedia of Planetary Science*

Mahaffy, P. R., Niemann, H. B., Alpert, A., Atreya, S. K., Demick, J., Donahue, T. M., Harpold, D. N. and Owen, T. C., 2000. Noble gas abundance and isotope ratios in the atmosphere of Jupiter from the *Galileo* Probe Mass Spectrometer. *Journal of Geophysical Research*, 105, 15061–15072

Mahaffy, P. R. et al, 2013. Abundance and Isotopic Composition of Gases in the Martian Atmosphere from the Curiosity Rover. *Science*, 341, 263–266

Marcq, E., Encrenaz, T., Bézard, B. and Birlan, M., 2006. Remote sensing of Venus' lower atmosphere from ground-based IR spectroscopy: Latitudinal and vertical distribution of minor species. *Planetary & Space Science*, 54, 1360–1370

Marcq, E., Mills, F. P., Parkinson, C. D. and Vandaele, A. C., 2018. Composition and Chemistry of the Neutral Atmosphere of Venus. *Space Science Reviews*, 214, 10

Marley, M. S. and Fortney, J. J., 2007. *Interiors of the Giant Planets*. 403–418

Marov, M. Y., 2004. Mikhail lomonosov and the discovery of the atmosphere of venus during the 1761 transit. *Proceedings of the International Astronomical Union*, 2004, 209–219

Marty, B., 2012. The origins and concentrations of water, carbon, nitrogen and noble gases on Earth. *Earth and Planetary Science Letters*, 313, 56–66. `1405.6336`

Mazor, E., Heymann, D. and Anders, E., 1970. Noble gases in carbonaceous chondrites. *Geochimica et Cosmochimica Acta*, 34, 781–824

McElroy, M. B. and Donahue, T. M., 1972. Stability of the Martian Atmosphere. *Science*, 177, 986–988

McGrath, M. A., Lellouch, E., Strobel, D. F., Feldman, P. D. and Johnson, R. E., 2004. *Satellite atmospheres*, volume 1. 457–483

Merkel, A. W., Cassidy, T. A., Vervack, R. J., McClintock, W. E., Sarantos, M., Burger, M. H. and Killen, R. M., 2017. Seasonal variations of Mercury's magnesium dayside exosphere from MESSENGER observations. *Icarus*, 281, 46–54

Mills, F. P., Esposito, L. W. and Yung, Y. L., 2007. Atmospheric composition, chemistry, and clouds. *Washington DC American Geophysical Union Geophysical Monograph Series*, 176, 73–100

Mills, F. P., Marcq, E., Yung, Y., Parkinson, C. D., Jessup, K. L. and Vandaele, A. C., 2019. Atmospheric Chemistry on Venus: An Overview of Unresolved Issues. In *Lunar and Planetary Science Conference*, Lunar and Planetary Science Conference. 2374

Montmessin, F., Bertaux, J.-L., Quémerais, E., Korablev, O., Rannou, P., Forget, F., Perrier, S., Fussen, D., Lebonnois, S., Rébérac, A. and Dimarellis, E., 2006. Subvisible CO $_2$ ice clouds detected in the mesosphere of Mars. *Icarus*, 183, 403–410

Morbidelli, A., Chambers, J., Lunine, J. I., Petit, J. M., Robert, F., Valsecchi, G. B. and Cyr, K. E., 2000. Source regions and time scales for the delivery of water to Earth. *Meteoritics and Planetary Science*, 35, 1309–1320

Moroz, V. I. and Zasova, L. V., 1997. VIRA-2: a review of inputs for updating the Venus International Reference Atmosphere. *Advances in Space Research*, 19, 1191–1201

Moses, J. I., Allen, M. and Yung, Y. L., 1992. Hydrocarbon nucleation and aerosol formation in Neptune's atmosphere. *Icarus*, 99, 318–346

Moses, J. I., Bézard, B., Lellouch, E., Gladstone, G. R., Feuchtgruber, H. and Allen, M., 2000. Photochemistry of Saturn's atmosphere. I. Hydrocarbon chemistry and comparisons with ISO observations. *Icarus*, 143, 244–298

Moses, J. I., Cavalie, T., Fletcher, L. N. and Roman, M. T., 2020. Atmospheric chemistry on Uranus and Neptune. *arXiv e-prints*, arXiv:2006.11367. `2006.11367`

Moses, J. I., Fletcher, L. N., Greathouse, T. K., Orton, G. S. and Hue, V., 2018. Seasonal stratospheric photochemistry on Uranus and Neptune. *Icarus*, 307, 124–145. `1803.10338`

Moses, J. I., Fouchet, T., Bézard, B., Gladstone, G. R., Lellouch, E. and Feuchtgruber, H., 2005. Photochemistry and diffusion in Jupiter's stratosphere: Constraints from ISO observations and comparisons with other giant planets. *Journal of Geophysical Research (Planets)*, 110, 8001

Moses, J. I., Rages, K. and Pollack, J. B., 1995. An analysis of Neptune's stratospheric haze using high-phase-angle voyager images. *Icarus*, 113, 232–266

Mueller, R. F., 1963. Chemistry and Petrology of Venus: Preliminary Deductions. *Science*, 141, 1046–1047

Mueller, R. F., 1964. A Chemical Model for the Lower Atmosphere of Venus. *Icarus*, 3, 285–298

Mumma, M. J., Villanueva, G. L., Novak, R. E., Hewagama, T., Bonev, B. P., DiSanti, M. A., Mandell, A. M. and Smith, M. D., 2009. Strong Release of Methane on Mars in Northern Summer 2003. *Science*, 323, 1041

Nair, H., Allen, M., Anbar, A. D., Yung, Y. L. and Clancy, R. T., 1994. A Photochemical Model of the Martian Atmosphere. *Icarus*, 111, 124–150

Navarro-González, R., Vargas, E., de la Rosa, J., Raga, A. C. and McKay, C. P., 2010. Reanalysis of the Viking results suggests perchlorate and organics at midlatitudes on Mars. *Journal of Geophysical Research (Planets)*, 115, E12010

NOAA/NASA/USAF, 1976. U.S. Standard Atmosphere, 1976. *NASA-TM-X-74335, NOAA-S/T-76-1562*

Norrish, R. G. W. and Wayne, R. P., 1965a. The Photolysis of Ozone by Ultraviolet Radiation. I. The Photolysis of Pure, Dry Ozone. *Proceedings of the Royal Society of London Series A*, 288, 200–211

Norrish, R. G. W. and Wayne, R. P., 1965b. The Photolysis of Ozone by Ultraviolet Radiation. II. The Photolysis of Ozone Mixed With Certain Hydrogen-Containing Substances. *Proceedings of the Royal Society of London Series A*, 288, 361–370

O'Brien, D. P., Izidoro, A., Jacobson, S. A., Raymond, S. N. and Rubie, D. C., 2018. The Delivery of Water During Terrestrial Planet Formation. *Space Science Reviews*, 214, 47. `1801.05456`

Oyama, V. I. and Berdahl, B. J., 1977. The Viking gas exchange experiment results from Chryse and Utopia surface samples. *Journal of Geophysical Research*, 82, 4669–4676

Pearl, J. C., Conrath, B. J., Hanel, R. A., Pirraglia, J. A. and Coustenis, A., 1990. The albedo, effective temperature, and energy balance of Uranus, as determined from Voyager IRIS data. *Icarus*, 84, 12–28

Pearl, J. C., Smith, M. D., Conrath, B. J., Bandfield, J. L. and Christensen, P. R., 2001. Observations of Martian ice clouds by the Mars Global Surveyor Thermal Emission Spectrometer: The first Martian year. *Journal of Geophysical Research*, 106, 12325–12338

Peebles, P. J. E., 1964. The structure and composition of Jupiter and Saturn. *Astrophsyical Journal*, 140, 328–+

Pepin, R. O., 1991. On the origin and early evolution of terrestrial planet atmospheres and meteoritic volatiles. *Icarus*, 92, 2–79

Pepin, R. O., 2006. Atmospheres on the terrestrial planets: Clues to origin and evolution. *Earth and Planetary Science Letters*, 252, 1–14

Plank, T. and Manning, C. E., 2019. Subducting carbon. *Nature*, 574, 343–352

Podolak, M., Hubbard, W. B. and Stevenson, D. J., 1991. *Models of Uranus' interior and magnetic field.* 29–61

Pollack, J. B. and Black, D. C., 1982. Noble gases in planetary atmospheres: Implications for the origin and evolution of atmospheres. *Icarus*, 51, 169–198

Pollack, J. B., Colburn, D., Kahn, R., Hunter, J., van Camp, W., Carlston, C. E. and Wolf, M. R., 1977. Properties of aerosols in the Martian atmosphere, as inferred from Viking lander imaging data. *Journal of Geophysical Research*, 82, 4479–4496

Pollack, J. B., Kasting, J. F., Richardson, S. M. and Poliakoff, K., 1987. The case for a wet, warm climate on early Mars. *Icarus*, 71, 203–224

Potter, A. and Morgan, T., 1985. Discovery of Sodium in the Atmosphere of Mercury. *Science*, 229, 651–653

Potter, A. E. and Morgan, T. H., 1986. Potassium in the atmosphere of Mercury. *Icarus*, 67, 336–340

Prinn, R. G., 1971. Photochemistry of HCl and other minor constituents in the atmosphere of Venus. *Journal of Atmospheric Sciences*, 28, 1058–1068

Prinn, R. G. and Barshay, S. S., 1977. Carbon monoxide on Jupiter and implications for atmospheric convection. *Science*, 198, 1031–1034

Prinn, R. G. and Lewis, J. S., 1975. Phosphine on Jupiter and Implications for the Great Red Spot. *Science*, 190, 274–276

Ramsey, W. H., 1951. On the constitutions of the major planets. *Monthly Notices of the Royal Astronomical Society*, 111, 427

Read, P. L., Barstow, J., Charnay, B., Chelvaniththilan, S., Irwin, P. G. J., Knight, S., Lebonnois, S., Lewis, S. R., Mendonça, J. and Montabone, L., 2016. Global energy budgets and 'Trenberth diagrams' for the climates of terrestrial and gas giant planets. *Quarterly Journal of the Royal Meteorological Society*, 142, 703–720

Romani, P. N. and Atreya, S. K., 1988. Methane photochemistry and haze production on Neptune. *Icarus*, 74, 424–445

Roulston, M. S. and Stevenson, D. J., 1995. Prediction of neon depletion in Jupiter's atmosphere. *EOS Transactions*, 76, 343

Sano, Y., Takahata, N., Nishio, Y., Fischer, T. P. and Williams, S. N., 2001. Volcanic flux of nitrogen from the Earth. *Chemical Geology*, 171, 263–271

Scheller, E. L., Ehlmann, B. L., Hu, R., Adams, D. J. and Yung, Y. L., 2021. Long-term drying of Mars by sequestration of ocean-scale volumes of water in the crust. *Science*, 372, 56–62

Schofield, J. T., Barnes, J. R., Crisp, D., Haberle, R. M., Larsen, S., Magalhães, J. A., Murphy, J. R., Seiff, A. and Wilson, G., 1997. The mars pathfinder atmospheric structure investigation/meteorology (asi/met) experiment. *Science*, 278, 1752–1758. `https://science.sciencemag.org/content/278/5344/1752.full.pdf`

Seiff, A. and Kirk, D. B., 1977. Structure of the atmosphere of Mars in summer at mid-latitudes. *Journal of Geophysical Research*, 82, 4364–4378

Seiff, A., Kirk, D. B., Knight, T. C. D., Young, R. E., Mihalov, J. D., Young, L. A., Milos, F. S., Schubert, G., Blanchard, R. C. and Atkinson, D., 1998. Thermal structure of Jupiter's atmosphere near the edge of a 5-μm hot spot in the north equatorial belt. *Journal of Geophysical Research*, 103, 22857–22890

Seiff, A., Schofield, J. T., Kliore, A. J., Taylor, F. W., Limaye, S. S., Revercomb, H. E., Sromovsky, L. A., Kerzhanovich, V. V., Moroz, V. I. and Marov, M. Y., 1985. Models of the structure of the atmosphere of Venus from the surface to 100 kilometers altitude. *Advances in Space Research*, 5, 3–58

Sill, G. T., 1972. Sulfuric acid in the Venus clouds. *Communications of the Lunar and Planetary Laboratory*, 9, 191–198

Slipher, V. M., 1904. The Lowell Spectrograph. *Astrophysical Journal*, 20, 1

Smith, B. A. et al, 1989. Voyager 2 at Neptune: Imaging Science Results. *Science*, 246, 1422–1449

Spencer, J. R., Stansberry, J. A., Trafton, L. M., Young, E. F., Binzel, R. P. and Croft, S. K., 1997. *Volatile Transport, Seasonal Cycles, and Atmospheric Dynamics on Pluto*. 435

Spiga, A., 2019. The Planetary Boundary Layer of Mars. *Oxford Research Encyclopedia of Planetary Science*, 130

Stevenson, D. J., 1982. Interiors of the Giant Planets. *Annual Review of Earth and Planetary Sciences*, 10, 257

Stewart, A. I., Anderson, D. E., Esposito, L. W. and Barth, C. A., 1979. Ultraviolet Spectroscopy of Venus: Initial Results from the Pioneer Venus Orbiter. *Science*, 203, 777–779

Stone, E. C. and Miner, E. D., 1989. The Voyager 2 Encounter with the Neptunian System. *Science*, 246, 1417–1421

Summers, M. E. and Strobel, D. F., 1989. Photochemistry of the Atmosphere of Uranus. *Astrophysical Journal*, 346, 495

Summers, M. E., Strobel, D. F. and Gladstone, G. R., 1997. *Chemical Models of Pluto's Atmosphere*. 391

Taylor, F. W., Atreya, S. K., Encrenaz, T., Hunten, D. M., Irwin, P. G. J. and Owen, T. C., 2004. The composition of the atmosphere of Jupiter. In *Jupiter. The Planet, Satellites and Magnetosphere* (F. Bagenal, T. E. Dowling, & W. B. McKinnon, eds.). Cambridge: Cambridge Univ. Press, 59–78

Teanby, N. A., Irwin, P. G. J. and Moses, J. I., 2019. Neptune's carbon monoxide profile and phosphine upper limits from Herschel/SPIRE: Implications for interior structure and formation. *Icarus*, 319, 86–98

Thomas, N. C., 1991. The early history of spectroscopy. *Journal of Chemical Education*, 68, 631. `https://doi.org/10.1021/ed068p631`

Titov, D. V., Ignatiev, N. I., McGouldrick, K., Wilquet, V. and Wilson, C. F., 2018. Clouds and Hazes of Venus. *Space Science Reviews*, 214, 126

Trafton, L., 1981. The atmospheres of the outer planets and satellites. *Reviews of Geophysics and Space Physics*, 19, 43–89

Trainer, M. G., Wong, M. H., McConnochie, T. H., Franz, H. B., Atreya, S. K., Conrad, P. G., Lefèvre, F., Mahaffy, P. R., Malespin, C. A., Manning, H. L. K., Martín-Torres, J., Martínez, G. M., McKay, C. P., Navarro-González, R., Vicente-Retortillo, Á., Webster, C. R. and Zorzano, M.-P., 2019. Seasonal Variations in Atmospheric Composition as Measured in Gale Crater, Mars. *Journal of Geophysical Research (Planets)*, 124, 3000–3024

Trieloff, M., 2017. Noble Gases. *Oxford Research Encyclopedia of Planetary Science*, 30

Urey, H. C., 1951. The origin and development of the earth and other terrestrial planets. *Geochimica et Cosmochimica Acta*, 1, 209–277

Vandaele, A. C., 2020. Composition and Chemistry of the Neutral Atmosphere of Venus. *Oxford Research Encyclopedia of Planetary Science*

Vervack, R. J., McClintock, W. E., Killen, R. M., Sprague, A. L., Anderson, B. J., Burger, M. H., Bradley, E. T., Mouawad, N., Solomon, S. C. and Izenberg, N. R., 2010. Mercury's Complex Exosphere: Results from MESSENGER's Third Flyby. *Science*, 329, 672

Villanueva, G. L., Mumma, M. J., Novak, R. E., Radeva, Y. L., Käufl, H. U., Smette, A., Tokunaga, A., Khayat, A., Encrenaz, T. and Hartogh, P., 2013. A sensitive search for organics (CH_4, CH_3OH, H_2CO, C_2H_6, C_2H_2, C_2H_4), hydroperoxyl (HO_2), nitrogen compounds (N_2O, NH_3, HCN) and chlorine species (HCl, CH_3Cl) on Mars using ground-based high-resolution infrared spectroscopy. *Icarus*, 223, 11–27

Visscher, C., 2020. Mapping Jupiter's Mischief. *Journal of Geophysical Research (Planets)*, 125, e06526

Visscher, C. and Fegley, B., Jr., 2005. Chemical constraints on the water and total oxygen abundances in the deep atmosphere of Saturn. *Astrophysical Journal*, 623, 1221–1227

Visscher, C., Lodders, K. and Fegley, B., Jr., 2006. Atmospheric Chemistry in Giant Planets, Brown Dwarfs, and Low-Mass Dwarf Stars. II. Sulfur and Phosphorus. *Astrophysical Journal*, 648, 1181–1195. `astro-ph/0511136`

Visscher, C., Lodders, K. and Fegley, B., Jr., 2010a. Atmospheric Chemistry in Giant Planets, Brown Dwarfs, and Low-mass Dwarf Stars. III. Iron, Magnesium, and Silicon. *Astrophysical Journal*, 716, 1060–1075. `1001.3639`

Visscher, C. and Moses, J. I., 2011. Quenching of Carbon Monoxide and Methane in the Atmospheres of Cool Brown Dwarfs and Hot Jupiters. *Astrophysical Journal*, 738, 72

Visscher, C., Moses, J. I. and Saslow, S. A., 2010b. The Deep Water Abundance on Jupiter: New Constraints from Thermochemical Kinetics and Diffusion Modeling. *Icarus*, 209, 602–615

Visscher, C., Sperier, A. D., Moses, J. I. and Keane, T. C., 2009. Phosphine and Ammonia Photochemistry in Jupiter's Troposphere. In *Lunar and Planetary Institute Science Conference Abstracts*, volume 40. 1201

von Zahn, U., Kumar, S., Niemann, H. and Prinn, R., 1983. *Composition of the Venus atmosphere*. 299

Wahl, S. M., Hubbard, W. B., Militzer, B., Guillot, T., Miguel, Y., Movshovitz, N., Kaspi, Y., Helled, R., Reese, D., Galanti, E., Levin, S., Connerney, J. E. and Bolton, S. J., 2017. Comparing Jupiter interior structure models to Juno gravity measurements and the role of a dilute core. *Geophysical Research Letters*, 44, 4649–4659. `1707.01997`

Wang, D., Lunine, J. I. and Mousis, O., 2016. Modeling the disequilibrium species for Jupiter and Saturn: Implications for Juno and Saturn entry probe. *Icarus*, 276, 21–38. `1604.06371`

Wayne, R., 2000. *Chemistry of Atmospheres: An Introduction to the Chemistry of the Atmospheres of Earth, the Planets, and Their Satellites*. Oxford University Press

Webster, C. R., Mahaffy, P. R., Atreya, S. K. et al, 2013. Low Upper Limit to Methane Abundance on Mars. *Science*, 342, 355–357

Webster, C. R., Mahaffy, P. R., Atreya, S. K. et al, 2015. Mars methane detection and variability at Gale crater. *Science*, 347, 415–417

Webster, C. R., Mahaffy, P. R., Atreya, S. K., Moores, J. E., Flesch, G. J., Malespin, C., McKay, C. P., Martinez, G., Smith, C. L., Martin-Torres, J., Gomez-Elvira, J., Zorzano, M.-P., Wong, M. H., Trainer, M. G., Steele, A., Archer, D., Sutter, B., Coll, P. J., Freissinet, C., Meslin, P.-Y., Gough, R. V., House, C. H., Pavlov, A., Eigenbrode, J. L., Glavin, D. P., Pearson, J. C., Keymeulen, D., Christensen, L. E., Schwenzer, S. P., Navarro-Gonzalez, R., Pla-García, J., Rafkin, S. C. R., Vicente-Retortillo, Á., Kahanpää, H., Viudez-Moreiras, D., Smith, M. D., Harri, A.-M., Genzer, M., Hassler, D. M., Lemmon, M., Crisp, J., Sander, S. P., Zurek, R. W. and Vasavada, A. R., 2018. Background levels of methane in Mars' atmosphere show strong seasonal variations. *Science*, 360, 1093–1096

Weidenschilling, S. J. and Lewis, J. S., 1973. Atmospheric and cloud structures of the jovian planets. *Icarus*, 20, 465–476

Wernicke, L. J. and Jakosky, B. M., 2021. Martian Hydrated Minerals: A Significant Water Sink. *Journal of Geophysical Research (Planets)*, 126, e06351

West, R. A., Baines, K. H., Friedson, A. J., Banfield, D., Ragent, B. and Taylor, F. W., 2007. Jovian clouds and haze. In *Jupiter. The Planet, Satellites and Magnetosphere* (F. Bagenal, T. E. Dowling, & W. B. McKinnon, eds.). Cambridge: Cambridge Univ. Press, 79–104

West, R. A., Baines, K. H. and Pollack, J. B., 1991. *Clouds and aerosols in the Uranian atmosphere.* 296–324

Whiteway, J. A., Komguem, L., Dickinson, C., Cook, C., Illnicki, M., Seabrook, J., Popovici, V., Duck, T. J., Davy, R., Taylor, P. A., Pathak, J., Fisher, D., Carswell, A. I., Daly, M., Hipkin, V., Zent, A. P., Hecht, M. H., Wood, S. E., Tamppari, L. K., Renno, N., Moores, J. E., Lemmon, M. T., Daerden, F. and Smith, P. H., 2009. Mars Water-Ice Clouds and Precipitation. *Science*, 325, 68

Wigner, E. and Huntington, H. B., 1935. On the Possibility of a Metallic Modification of Hydrogen. *Journal of Chemical Physics*, 3, 764–770

Wildt, R., 1932. Absorptionsspektren und Atmosphären der gros;en Planeten. *Veroeffentlichungen der Universitaets-Sternwarte zu Goettingen*, 2, 171

Wildt, R., 1940. Note on the Surface Temperature of Venus. *Astrophysical Journal*, 91, 266–268

Winick, J. R. and Stewart, A. I. F., 1980. Photochemistry of SO2 in Venus' upper cloud layers. *Journal of Geophysical Research*, 85, 7849–7860

Wong, M. H., Mahaffy, P. R., Atreya, S. K., Niemann, H. B. and Owen, T. C., 2004. Updated *Galileo* probe mass spectrometer measurements of carbon, oxygen, nitrogen, and sulfur on Jupiter. *Icarus*, 171, 153–170

Wurz, P., Rohner, U., Whitby, J. A., Kolb, C., Lammer, H., Dobnikar, P. and Martín-Fernández, J. A., 2007. The lunar exosphere: The sputtering contribution. *Icarus*, 191, 486–496

Yelle, R. V. and Elliot, J. L., 1997. *Atmospheric Structure and Composition: Pluto and Charon*. 347

Yelle, R. V. and McGrath, M. A., 1996. Ultraviolet Spectroscopy of the SL9 Impact Sites. *Icarus*, 119, 90–111

Young, A. T., 1973. Are the Clouds of Venus Sulfuric Acid? *Icarus*, 18, 564–582

Yung, Y. L. and Demore, W. B., 1982. Photochemistry of the stratosphere of Venus: Implications for atmospheric evolution. *Icarus*, 51, 199–247

Yung, Y. L. and DeMore, W. B., 1999. *Photochemistry of Planetary Atmospheres*. New York: Oxford Univ. Press

Zahnle, K., Freedman, R. S. and Catling, D. C., 2011. Is there methane on Mars? *Icarus*, 212, 493–503

Zalucha, A. M. and Cook, J., 2019. *The Structure and Dynamics of the Atmospheres of Pluto and Triton*. 113

Zhang, J., Dauphas, N., Davis, A. M., Leya, I. and Fedkin, A., 2012. The proto-Earth as a significant source of lunar material. *Nature Geoscience*, 5, 251–255

Zolotov, M., 2019. Chemical Weathering on Venus. *Oxford Research Encyclopedia of Planetary Science*, 146

Zolotov, M. Y., 2018. Gas-Solid Interactions on Venus and Other Solar System Bodies. *Reviews in Mineralogy and Geochemistry*, 84, 351–392